npj | materials degradation

Article

Published in partnership with CSCP and USTB

https://doi.org/10.1038/s41529-025-00674-8

Establishing a pre-passivation method to improve the corrosion resistance of B30 alloy in deep-sea environment

Tengfei Yin, Song Meng, Yang Zhao ✉, Tao Zhang & Fuhui Wang

The response surface methodology (RSM) was used to investigate the influence of benzotriazole (BTA), sulfosalicylic acid (SSA), H_2O_2, and temperature on the corrosion resistance of pre-passivation film formed on copper. The optimal pre-passivation process was predicted: BTA of 14–16 g/L, SSA of 2–2.3 g/L, H_2O_2 of 10–11 ml/L, sodium dodecylsulfate of 0.5 g/L and temperature of 45–50 °C. An improved pre-passivation treatment suitable for B30 alloy, using H_3PO_4 instead of SSA, showed good corrosion resistance; the polarization resistance increased nearly 100 times in its 'infancy'. In the 30 days of corrosion test, the localized corrosion was significantly inhibited, thus prolonging the service life of the heat-transfer tube.

Nowadays, human society is facing the challenges of continuous population expansion, increasing shortage of natural resources and rapid deterioration of ecological environment. The global attention is focused on the ocean, and efforts are made to promote the development and comprehensive utilization of marine resources. The deep-sea environment is extremely harsh, with a low temperature, low oxygen, high pressure, and high salinity[1]. This aggressive environment poses a great threat to the safe use of metal materials[2].

As the core component of the power system, heat exchanger directly affects the stable operation of marine equipment[3]. 70/30 copper-nickel alloy (B30) has excellent thermal conductivity, corrosion resistance, and anti-fouling performance, and is the ideal material for heat-transfer tubes[4]. When B30 alloy is immersed in seawater for more than a critical time, the corrosion resistance of the alloy significantly improves. The stage before this critical time is called 'infancy'. The excellent corrosion resistance of B30 alloy is attributed to the formation of protective multilayers on its surface during its 'infancy'[5,6]. The inner layer is composed of dense Cu_2O. The doping of Ni and Fe into Cu_2O reduces the defect density of the passivation film, which plays a key role in its excellent corrosion resistance[7,8]. The outer layer is composed of amorphous γ-FeOOH and loose Cu^{2+} products[9,10] to protect the thermodynamic stability of the inner layer. However, a large number of cases of power system failures caused by heat-transfer tube leakage have been reported, which can be attributed to the loose and unprotected corrosion product film formed in the 'infancy' in the aggressive environment[11–13]. Therefore, it is very important to explore an efficient pretreatment method to ensure the effective survival of B30 alloy in its 'infancy' stage and form a more protective film for prolonging the service life of a power system[14].

So far, scientists have done a lot of research on the pretreatment methods of copper alloys. Plasma electrolytic oxidation (PEO) is a common pretreatment method for Cu alloys[15]. PEO combined with other post-treatment processes, such as high-temperature oxidation, silane coupling agent mixed with benzotriazole (BTA), showed better corrosion resistance and adhesion strength[16]. Due to its unique film-forming mechanism, PEO coatings often have pores and microcracks, which are not suitable for workpieces with complex shapes. Scientists also found that a thick FeOOH/Fe_2O_3 layer was formed in $FeSO_4$ solution, which changed the main carrier type of semiconductor film as well as the cathodic electrode process[17], thus inhibiting the corrosion of copper alloy in NaCl solution[18] and polluted seawater[19]. Although this method has a low cost and a good treatment effect, its application is limited due to poor environmental protection and poor stability of the treatment solution. The corrosion resistance of copper alloy has also been improved by immersing in inorganic metal salts, such as chromate[20] and phosphate[21] and depositing a dense protective film on the substrate through chemical reaction. Although inorganic passivation is simple and convenient, it is prohibited for use in some countries because of its high toxicity and environmental protection. In addition, scientists also tried to form in-situ corrosion film on the surface of copper alloy by pre-immersing treatment in Cl^- containing medium[22]. The existing research results believe that it is beneficial to form the film with excellent corrosion resistance in the environment of high temperature[10], aeration[23], and dynamic flow[14]. Unfortunately, the efficiency of this method is relatively low, and the protective film can be formed after at least 20 days of pre-immersion treatment. In view of the shortcomings of the existing copper alloy pre-treatment methods, there is a lack of fast, simple, highly protective and environmentally friendly pretreatment methods.

Recently, organic passivation treatment (corrosion inhibitor) has developed rapidly, with the advantages of low toxicity, low pollution, good corrosion resistance and good self-healing[24]. Heterocyclic organic compounds containing nitrogen[25–27], oxygen[28], sulfur[29–32] and/or aromatic rings are considered to be the most promising inhibitors. A large number of studies have shown that the sulfur and nitrogen parts of the corrosion inhibitor compounds provide lone pair electrons and form coordination bonds with Cu, Cu^+, or Cu^{2+} species, thus forming a protective complex on

The State Key Laboratory of Digital Steel, Northeastern University, Shenyang, P.R. China. ✉e-mail: zhaoyang7402@mail.neu.edu.cn

the metal surface, which plays a key role in protecting the alloy from corrosion damage[33,34]. Among all corrosion inhibitors, BTA and its derivatives have been developed for more than 70 years[35]. It is considered to be an effective corrosion inhibitor for copper and its alloys, such as relieving stress corrosion cracking and flow accelerated corrosion of brass[36,37], and atmospheric corrosion of pure copper[38]. Kosec et al.[39] found that the polarization resistance (R_p) increased with the increase of BTA concentration, exhibiting better corrosion resistance. They proposed that the structure of the protective layer can be stabilized either as Cu2O and Cu(I)BTA as the lower layer and the upper layer, or the composition of Cu2O and Cu(I)BTA is in the protective layer. Tromans[40] believed that the thermodynamic stability of Cu(I)BTA complex is better than that of Cu_2O, so Cu(I)BTA complex is beneficial to maintain the stability of Cu_2O. A large number of studies have found that the corrosion inhibition effect of the compound BTA passivation system is better than that of a single BTA passivation system[41,42]. Villamil et al.[43,44] found that BTA and sodium dodecylsulfate (SDS) can synergistically inhibit copper corrosion in sulfuric acid media. SDS can not only reduce the surface tension of BTA molecules on the metal surface, but also adsorb on the copper surface to form dodecylsulfate ions. Yang et al.[24] found that Cu and its alloy had a faster film-formation rate in BTA-H_2O_2 solution, exhibiting excellent corrosion resistance. Liao et al.[45] found that when BTA and $CeCl_3$ are added together, CeO_2, $Ce(OH)_3$, or the complex formed by Ce and BTA were deposited on the surface of copper alloy. This passivation film is compact, which enhances the bonding strength between the film and the substrate and improves the corrosion inhibition performance. In addition, BTA and sulfosalicylic acid (SSA) also have a synergistic effect in improving the corrosion inhibition effect[46]. The corrosion resistance of the passivation film prepared by the composite passivant containing BTA and SSA is better than that of the single BTA passivant. After a systematic review of the above studies, three key issues remain unclear. First of all, BTA is usually used in a closed environment as a corrosion inhibitor for copper and its alloys. When the passivation film is locally damaged, it can be repaired quickly. B30 heat-transfer tube is an open environment, so it is not suitable to use a corrosion inhibitor. Therefore, the pre-passivation treatment must be carried out before the heat-transfer tube is put into service. This kind of pre-passivation film cannot repair itself in the long-term service as in the closed environment containing corrosion inhibitor. Therefore, whether the film can help the alloy through its 'infancy' and form a compact regenerated film is the key to the success of pre-passivation treatment. At present, there is still a lack of relevant research. Second, B30 alloy mainly contains two components (Cu and Ni), and the composite pre-passivation system involves at least 3–5 variables. It is difficult to propose an efficient pre-passivation treatment process when considering alloy elements and multiple component pre-passivation system[47]. Third, most of the existing studies focus on the corrosion inhibition effect of BTA in mild environments (static, normal temperature, atmospheric pressure), and the lack of research on aggressive deep-sea environments may lead to the deviation of research conclusions.

The aim of this work is to propose a rapid, efficient and environmentally friendly pre-passivation treatment process for B30 alloy to prolong the service life of heat-transfer tubes used in the aggressive deep-sea environment. In addition, this work also provides a new perspective for understanding how the pre-passivation treatment can help B30 alloy safely survive its 'infancy' in the aggressive deep-sea environment.

Results and discussion

Design of pre-passivation system for B30 alloy

Nowadays, scientists have carried out a large number of research on BTA organic passivation of pure copper[23,30,32,34,38,41,42,44,45], brass[36,37,39,48] and bronze[24,49–53], but less research on BTA organic passivation of copper-nickel alloy. The content of Ni in B30 alloy is as high as 30%, so the role of Ni in the formation of the pre-passivation film should also be considered in the design of the B30 pre-passivation system. Considering the alloy factors (Cu, Ni) and the composite pre-passivation system, this work will become very complex. It is difficult to explain the influence mechanism of various factors and their interactions. Therefore, we first investigated the effects of various single factors and their interactions on the corrosion resistance of the pre-passivation film formed on pure copper based on RSM. According to the RSM analysis results, the optimal pre-passivation treatment process of pure copper was predicted. On this basis, an improved pre-passivation treatment process suitable for B30 alloy was proposed.

Table 1 | The isoelectric point of metal oxide and hydroxide particles

	$Ni(OH)_2$	$Cu(OH)_2$	NiO	CuO	Cu_2O
pH	2.87	7.44	9.48	5.67	10.54

Figure 1 shows the design of the pure copper and B30 alloy pre-passivation system. For the pre-passivation system of pure copper, BTA was selected as the main passivation agent. A large number of studies have found that H_2O_2 can improve the passivation effect of BTA and form films with better corrosion resistance[24,54,55]. H_2O_2 shows strong oxidation, which can accelerate the dissolution rate of pure copper matrix, thus forming more metal ions[56,57]. The higher the concentration of metal ions in the electrolyte, the greater the driving force for the deposition of the complex formed by metal and BTA, leading to the formation of a denser and thicker passivation film[58,59]. Kondoh et al.[60] found that the uncovered part of Cu-BTA was oxidized in the presence of H_2O_2, improving the integrity of the passivation film. Therefore, H_2O_2 was selected as the oxidant in this pre-passivation system. In addition, in the acidic environment containing H_2O_2, pure copper has a greater negative corrosion potential, resulting in an increase in the dissolution rate. In the chemical mechanical polishing process, scientists often combine acidifiers and H_2O_2 to accelerate the removal rate of copper and its alloys[57,61–63]. Wang et al.[46] studied the corrosion resistance of the organic passivation film formed in the composite pre-passivation system containing SSA. The research results indicate that SSA was involved in the formation of passivation film and exhibited a synergistic effect with BTA. Wang et al.[64] found that in the process of DNA electrochemical cutting, Cu forms [$Cu(ssal)_2^{2+}$] complex by complexing with SSA. Considering that SSA cannot only provide an acidic environment, but also complex with Cu, it was applied to the pre-passivation system of pure copper. Temperature is a key factor in the process of organic passivation, which not only affects passivation kinetics but also affects the stability of H_2O_2. Therefore, temperature is selected as one of the variables in the pre-passivation process. In addition, SDS was selected as the surfactant of the pre-passivation system. A large number of studies have found that SDS and BTA showed a synergistic effect in inhibiting Cu corrosion[43,44,65,66], and with the increase of SDS concentration, the wettability of copper and solution increases[67], thus improving the compactness and uniformity of the assivation film. Cui et al.[68] proposed a new inhibition mechanism to explain the effect of inhibitors on the nucleation of corrosion products. They believe that the corrosion inhibitor with opposite charge can neutralize the charge on the surface of the corrosion product embryo, so as to improve the nucleation rate. Consequently, much denser corrosion product film and excellent corrosion inhibition efficiency were obtained. Table 1 shows the isoelectric point measurement of metal oxide and hydroxide particles. In the acidic pre-passivation system, Cu_2O, CuO, NiO, $Cu(OH)_2$ particles are positively charged, while SDS with a negative charge can neutralize the positive charge on the surface of the above particles, thus promoting the formation of a dense oxide film. Because excessive addition of SDS will lead to serious foaming of the pre-passivation solution, even if a small amount of SDS is added, the surface tension will be significantly reduced[67], so the SDS in the pre-passivation system is 0.5 g/L.

For the pre-passivation system of B30 alloy, based on the following considerations, we use phosphoric acid instead of SSA as an acidifier: first, the copper alloy has better passivation performance in the medium containing phosphate ions, showing a higher pitting potential[23], thus reducing the pitting sensitivity[69]. Secondly, phosphoric acid[70] and phosphate[71] can promote the passivation of Ni and Fe, and $Ni_3(PO_4)_2$ and $FePO_4$ can act as heterogeneous nucleation sites to promote the

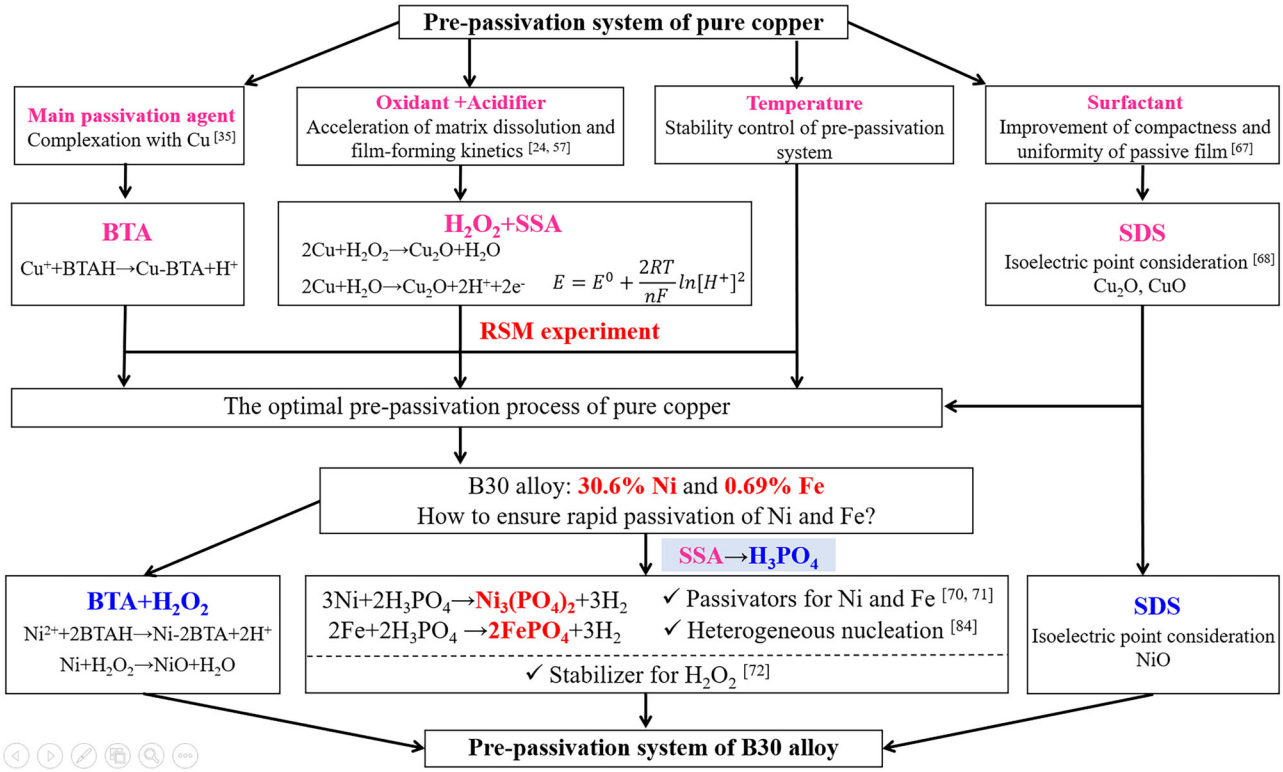

Fig. 1 | Design of the pre-passivation system of pure copper and B30 alloy.

Table 2 | Variance analysis of the regression model for E_{pit}

Source	Sum of squares	df	Mean square	*F* value	*P* value
Model	0.3528	14	0.0252	32.6	< 0.0001
A-BTA	0.1426	1	0.1426	184.51	< 0.0001
B-Sulfosalicylic acid	0.032	1	0.032	41.44	< 0.0001
C-H_2O_2	0.0399	1	0.0399	51.56	< 0.0001
D-Temperature	0.0005	1	0.0005	0.6981	0.4086
AB	0.0202	1	0.0202	26.12	< 0.0001
AC	0.0031	1	0.0031	4.05	0.0514
AD	0.0034	1	0.0034	4.43	0.0419
BC	0.0001	1	0.0001	0.1697	0.6827
BD	0.0001	1	0.0001	0.1889	0.6663
CD	0.0002	1	0.0002	0.2359	0.6300
A^2	0.0774	1	0.0774	100.14	< 0.0001
B^2	0.0107	1	0.0107	13.84	0.0006
C^2	0.0008	1	0.0008	0.9836	0.3276
D^2	0.0048	1	0.0048	6.15	0.0177
Residual	0.0294	38	0.0008		
Lack of Fit	0.0131	12	0.0011	1.74	0.1148
Pure Error	0.0163	26	0.0006		
Cor Total	0.3822	52			
R^2 = 0.9231, Adjusted R^2 = 0.8948, Predicted R^2 = 0.8469					

formation of the passivation film. Thirdly, phosphoric acid can effectively improve the stability of H_2O_2 and prevent the decomposition of H_2O_2 at higher temperatures[72]. In addition, other components in the B30 alloy pre-passivation system are the same as those in the pure copper pre-passivation system.

Pre-passivation treatment of pure copper and corrosion tests

Firstly, the pre-passivation treatment was conducted on pure copper under the process conditions listed in the RSM table (Table S1). Secondly, the potentiodynamic polarization curve of the sample after pre-passivation treatment was measured, and the results are shown in Fig. S1. Thirdly, pitting potential (E_{pit}) and passive current density (i_p) obtained by anodic polarization curves were filled in the RSM table, as shown in Table S1. The quadratic model with the highest power of the quadratic term showed the best fit, so this model was selected for analysis. The variance analysis of the response surface quadratic model, shown in Table 2 and Table S2 is used to analyze the influence degree of each factor. R^2 is close to 1, and the difference between the adjusted R^2 and predicted R^2 is <0.2 for different response values, indicating the high accuracy of the regression equation[73]. *F* value and *p* value are usually used to analyze the significance of various factors[74]. $p < 0.05$ indicates that a factor has a significant impact on the response value, and $p < 0.01$ indicates that a factor has an extremely significant impact on the response value. However, $p > 0.1$ indicates that a certain factor has no significant effect on the response value. For pitting potential (E_{pit}), the significant influence factors were: BTA (A/A^2), SSA (B/B^2), H_2O_2 (C), Temperature (D^2), BTA × SSA (AB), BTA × H_2O_2 (AC), and BTA × Temperature (AD). All interactions were related to BTA, which indicates that BTA was the most important influencing factor. The degree of influence decreased in the following order: BTA (A/A^2) > BTA × SSA (AB) > H_2O_2 (C) > SSA (B/B^2) > Temperature (D^2) > BTA × Temperature (AD) > BTA × H_2O_2 (AC). A simplified model considering only significant items is as follows:

$$E_{pit} = 0.225 + 0.077A - 0.037B - 0.041C + 0.051AB + 0.020AC - 0.021AD - 0.084A^2 - 0.032B^2 + 0.021D^2 \quad (1)$$

The factors that significantly affect the passive current density (i_p) are: BTA (A/A^2), SSA (B^2), H_2O_2 (C^2), BTA × SSA (AB) and BTA × H_2O_2 (AC). The

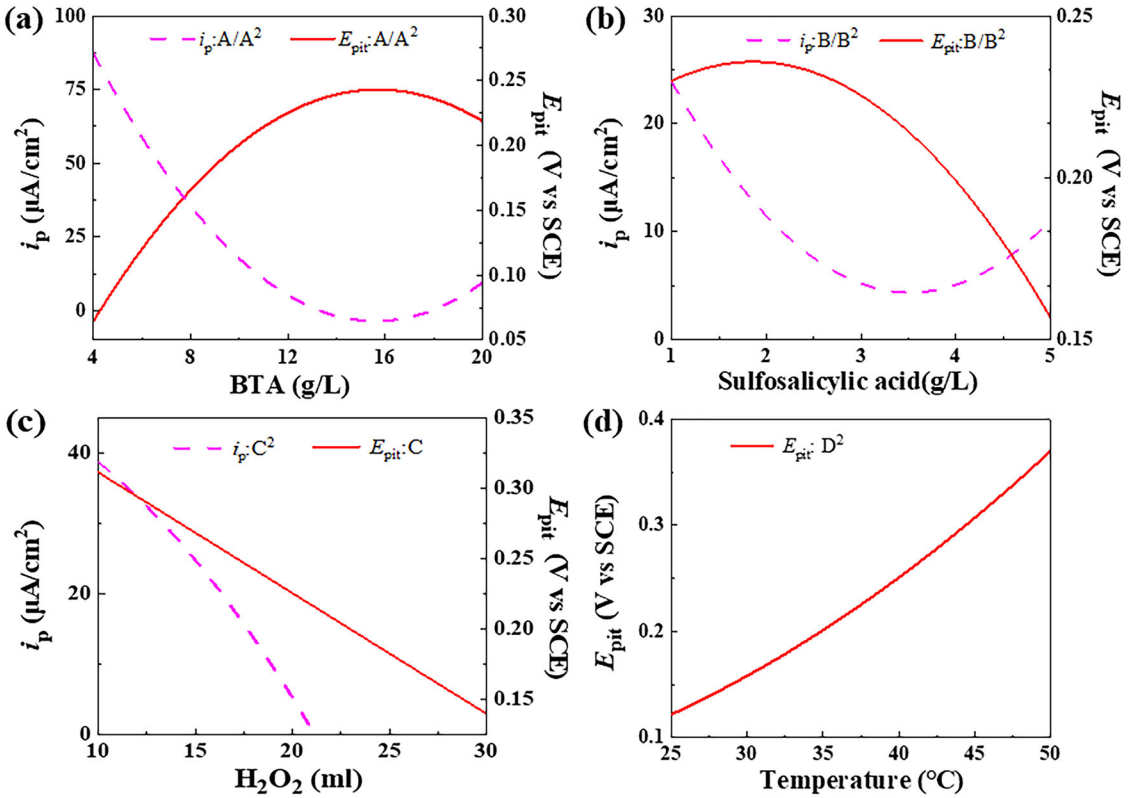

Fig. 2 | The impact curves of various single factors on the pitting potential (E_{pit}) and passive current density (i_p). **a** BTA, **b** SSA, **c** H_2O_2, **d** temperature.

degree of influence decreased in the following order: BTA (A/A^2) > SSA (B/B^2) > H_2O_2 (C^2) > BTA × SSA (AB) > BTA × H_2O_2 (AC). A simplified model considering only significant items was obtained as follows:

$$i_p = 5.187 - 38.848A - 6.408B - 12.44AB - 12.036AC + 43.128A^2 + 12.265B^2 - 11.177C^2 \quad (2)$$

Figure 2 shows the impact curves of various single factors on the corrosion resistance of the passivation film. Higher BTA concentration (14–17 g/L) is conducive to improving the corrosion resistance of passivation film, as shown in Fig. 2a. The optimal concentration range of SSA (B/B^2) is different for pitting potential (E_{pit}) and passive current density (i_p), as shown in Fig. 2b. Pitting potential can better reflect the stability of passivation film than passive current[75], and the optimal concentration range of SSA is 1.3-2.3 g/L. The optimal concentration range of H_2O_2 (C/C^2) was also different for E_{pit} and i_p, as shown in Fig. 2c. Considering E_{pit}, the optimal concentration range of H_2O_2 was 10–11 ml/L. E_{pit} increases with the increase of passivation temperature, so the optimal temperature range is 45–50 °C, as shown in Fig. 2d

Figure 3 show the 3D response surface and contour plots of the effect of the significant interaction term on E_{pit}. According to 3D response surface and contour plots between E_{pit} and BTA × SSA as shown in Fig. 3a, relatively high BTA and moderate SSA concentration promote the formation of protective film. The optimal ranges for these two factors were 10–16 g/L and 1–4 g/L. Acidic passivation solution accelerates the dissolution of pure copper and forms more metal ions[54]. When the metal ions are sufficient, the increase of BTA concentration promotes the formation kinetics of passivation film[58,59], thus providing better corrosion resistance. According to 3D response surface and contour plots between E_{pit} and BTA × H_2O_2 as shown in Fig. 3b, relatively high BTA and low H_2O_2 concentration promote the formation of protective film. H_2O_2 can accelerate the dissolution rate of copper and its alloys in an acidic environment. However, oxides are formed at higher H_2O_2 concentration, resulting in lower matrix dissolution rate and organic passivation film formation rate[57]. Therefore, the optimal concentration ranges of BTA and H_2O_2 are 12–18 g/L and 10–15 ml/L, respectively. Moreover, the dissolution of pure copper and the formation of passivation film conform to Arrhenius equation, so the above two processes are accelerated with the increase of pre-passivation temperature[76–79]. Because H_2O_2 decomposes easily at higher temperature, reducing the pre-passivation temperature is conducive to improving the stability of the pre-passivation solution. According to 3D response surface and contour plots between E_{pit} and BTA × Temperature shown in Fig. 3c, relatively high and low temperature are conducive to improving the corrosion resistance of the passivation film at high BTA concentration. The optimal ranges of these two factors were 12–20 g/L and 25–30/45–50 °C, respectively. Figure 4 shows the 3D response surface and contour plots of the impact of significant interaction items on i_p. Similar to Fig. 3a, in a wide range of SSA concentration, higher BTA concentration is conducive to improving the corrosion resistance of passivation film, and obtaining the minimum i_p, as shown in Fig. 4a. The optimal ranges of these two factors were 12–20 g/L and 2–5 g/L, respectively. There is a slight interaction between i_p and BTA × H_2O_2, as shown in Fig. 4b. The optimal ranges for these two factors are 12–18 g/L and 10-30 ml/L, respectively.

Considering the single factor and their interactions comprehensively, the optimal pre-passivation process for pure copper was determined by taking E_{pit} as the optimal response value: BTA concentration of 14-16 g/L, SSA concentration of 2–2.3 g/L, H_2O_2 concentration of 10–11 ml/L, SDS concentration of 0.5 g/L and temperature of 45–50 °C.

Figure 5 shows the potentiodynamic polarization curves of the bare sample and pre-passivation samples under the optimal process. Obvious passivation zone was observed in the anodic polarization curve after pre-passivation treatment, and the E_{pit} extended to 0.3 V (vs SCE), which was more positive than the E_{pit} value listed in Table S1. In contrast, no passivation phenomenon occurred in the bare sample, and the reduction of local current density in the anodic polarization curve was due to the formation of unprotected corrosion products on the substrate surface. Other scientists believed that this region corresponds to the formation of blue-green cupric

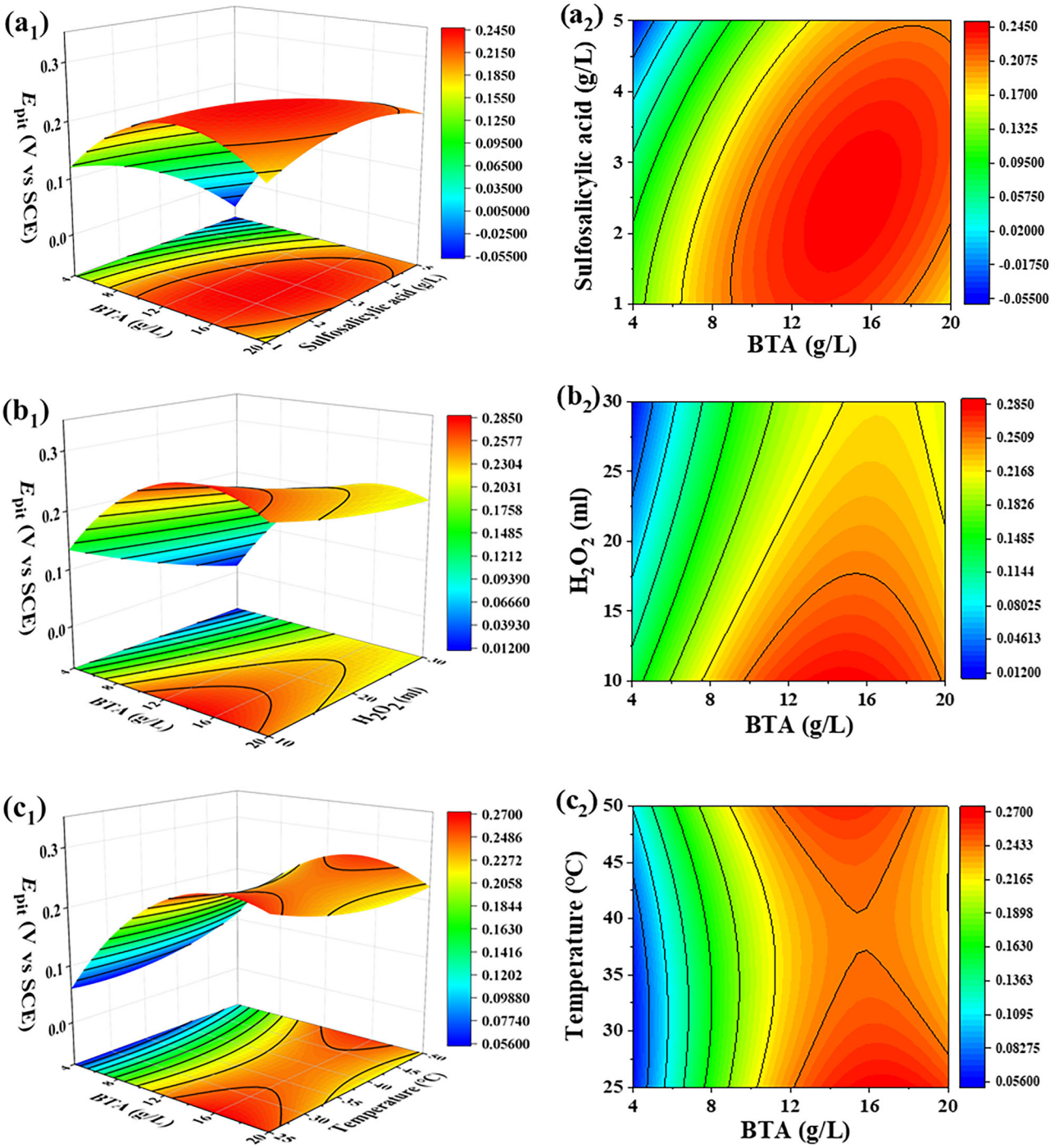

Fig. 3 | 3D response surface plots and contour plots for the impact of interactions on the pitting potential (E_{pit}). a BTA × sulfosalicylic acid, **b** BTA × H_2O_2, **c** BTA × temperature.

oxychloride[80]. Its coverage of the electrode surface temporarily delays the current density increase, which then continues further as the electrode potential becomes more positive. It can be seen that the passivation film formed under the optimal process exhibits the best corrosion resistance, and inhibits the corrosion of the substrate[35]. Figure 6 shows the electrochemical impedance spectrum of bare samples and pre-passivation samples immersed in artificial seawater at 25°C for 90 days. The equivalent circuits shown in Fig. 7 is used to fit the EIS data of bare copper samples and pre-passivation samples, where R_s is the solution resistance, Q_f is the constant phase element of the passivation film, R_f is the passivation film resistance, and Q_{dl} and R_{ct} are the constant phase elements of the electrical double layer and charge-transfer resistance, respectively. The fitted electrochemical parameters are listed in Table S3. In the Nyquist plots of the bare sample, the radius of the capacitance arc increases continuously within 20 days of immersion. Subsequently, with the extension of immersion time, the arc radius of the capacitance fluctuated continuously, indicating that the corrosion products were in a dynamic equilibrium of formation-dissolution-reformation. As can be seen from the Bode plot shown in Fig. 6(a2), the low-frequency |Z| values and maximum phase angles of the bare samples gradually increase with the extension of corrosion time, which indicates an increase in the corrosion resistance. Although the capacitance arc radius of pre-passivation samples also fluctuates continuously with the immersion time, considering the coordinate axis range, its radius is much larger than that of the bare sample, as shown in Fig. 6(b1). Similar to the capacitance arc radius, within

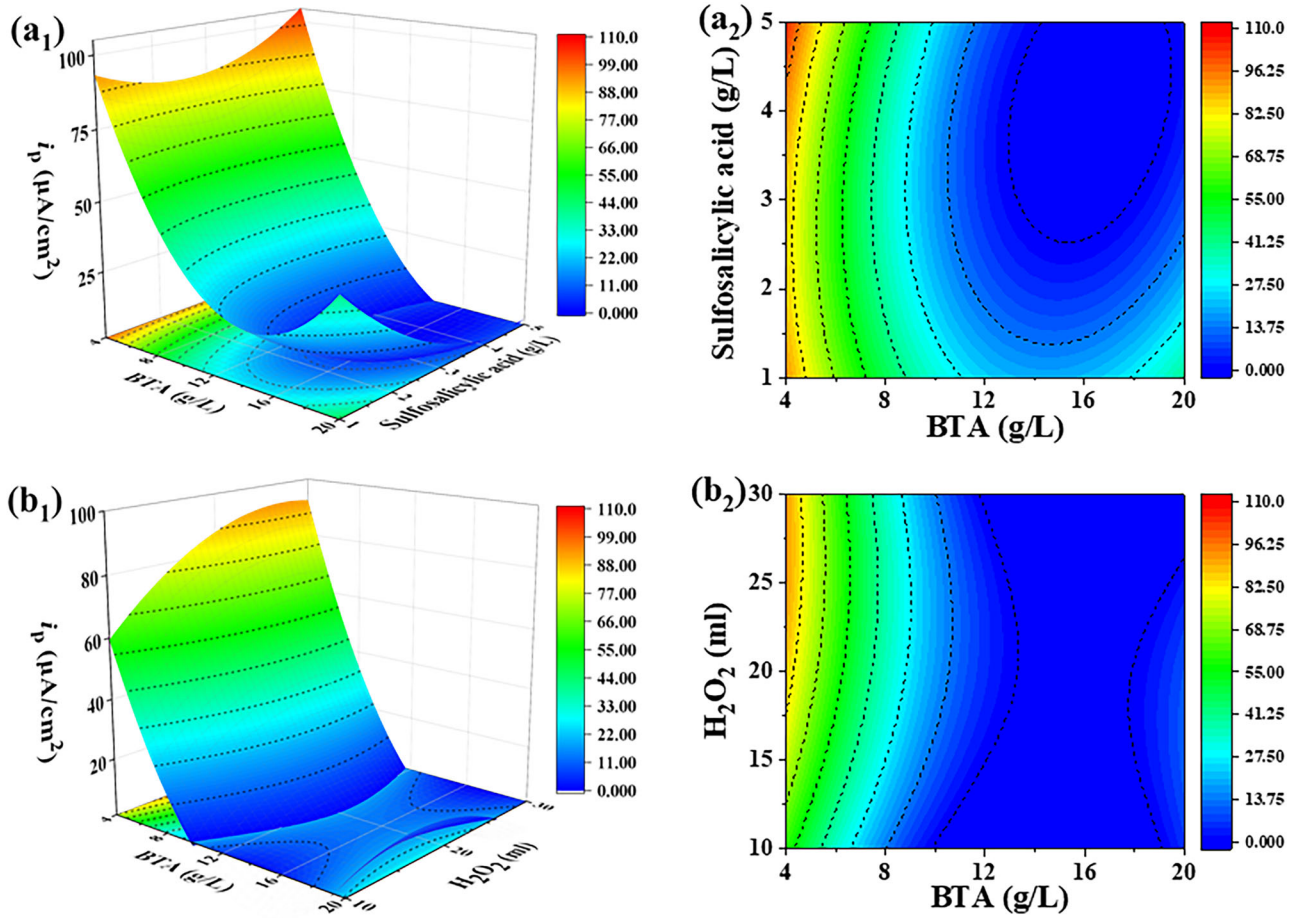

Fig. 4 | 3D response surface plots and contour plots for the impact of interactions on the pitting potential (E_{pit}). a BTA × sulfosalicylic acid, **b** BTA × H_2O_2.

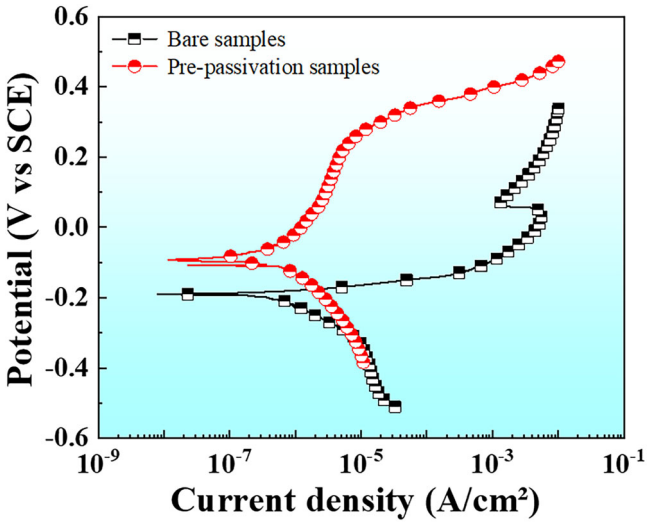

Fig. 5 | Potentiodynamic polarization curves of the bare copper samples and optimal pre-passivation samples.

the low-frequency range, the |Z| values fluctuate continuously with the immersion time. After 90 days of corrosion, the low-frequency |Z| value of the pre-passivation samples reaches its maximum value, which is one order of magnitude larger than that of the bare sample. According to the fitted electrochemical parameters shown in Table S3, the n_f, n_{ct}, and R_f values of the pre-passivation film are higher than those of bare samples, which indicates that the pre-passivation film is more compact than the corrosion product film on the bare samples and provides excellent protection. Figure 6c shows that the R_p of bare sample generally increases with the extension of immersion time, indicating the formation of corrosion products. In contrast, the R_p of pre-passivation samples decreased within 50 days of corrosion immersion. With the repair of passivation film, R_p increased continuously in the subsequent corrosion process, and reached the maximum after 90 days of corrosion. It is worth noting that the R_p of the pre-passivation samples is greater than that of the bare sample at each stage, and the R_p increased by about 3 orders of magnitude after 90 days of corrosion. The electrochemical test results indicate that passivation film formed under the optimal process conditions has excellent corrosion resistance.

Figure 8 shows the surface morphology before and after pre-passivation treatment under the optimal process. Before pre-passivation treatment, there are obvious wear marks on the surface of the pure copper substrate, as shown in Fig. 8a. The surface of copper substrate is covered with passivation film, and no wear trace is found after pre-passivation treatment, as shown in Fig. 8b.

Figure 9 shows the X-ray photoelectron spectroscopy (XPS) spectrum of the surface of the passivation film formed under the optimal process. The main components of the organic passivation film are Cu, O, C, N, and S. In the Cu 2p spectrum shown in Fig. 9b, Cu_2O, CuO, Cu(I)-BTA were detected in the passivation film. Cu(I)-BTA is the product of BTA complexation with Cu^+ in Cu_2O. Ling et al.[81] proposed that BTA was initially adsorbed on the positively charged Cu_2O surface through electrostatic interaction, and then formed a Cu(I)-BTA complex. The O 1 s spectrum also proves the existence of CuO and Cu_2O in the passivation film, as shown in Fig. 9c. In the S 2p spectrum shown in Fig. 9d, $-SO_3H^-$ from SSA was detected in the passivation film, indicating that SSA was also involved in the formation of passivation film. BTA and Cu(I)-BTA were detected in the N 1 s spectrum

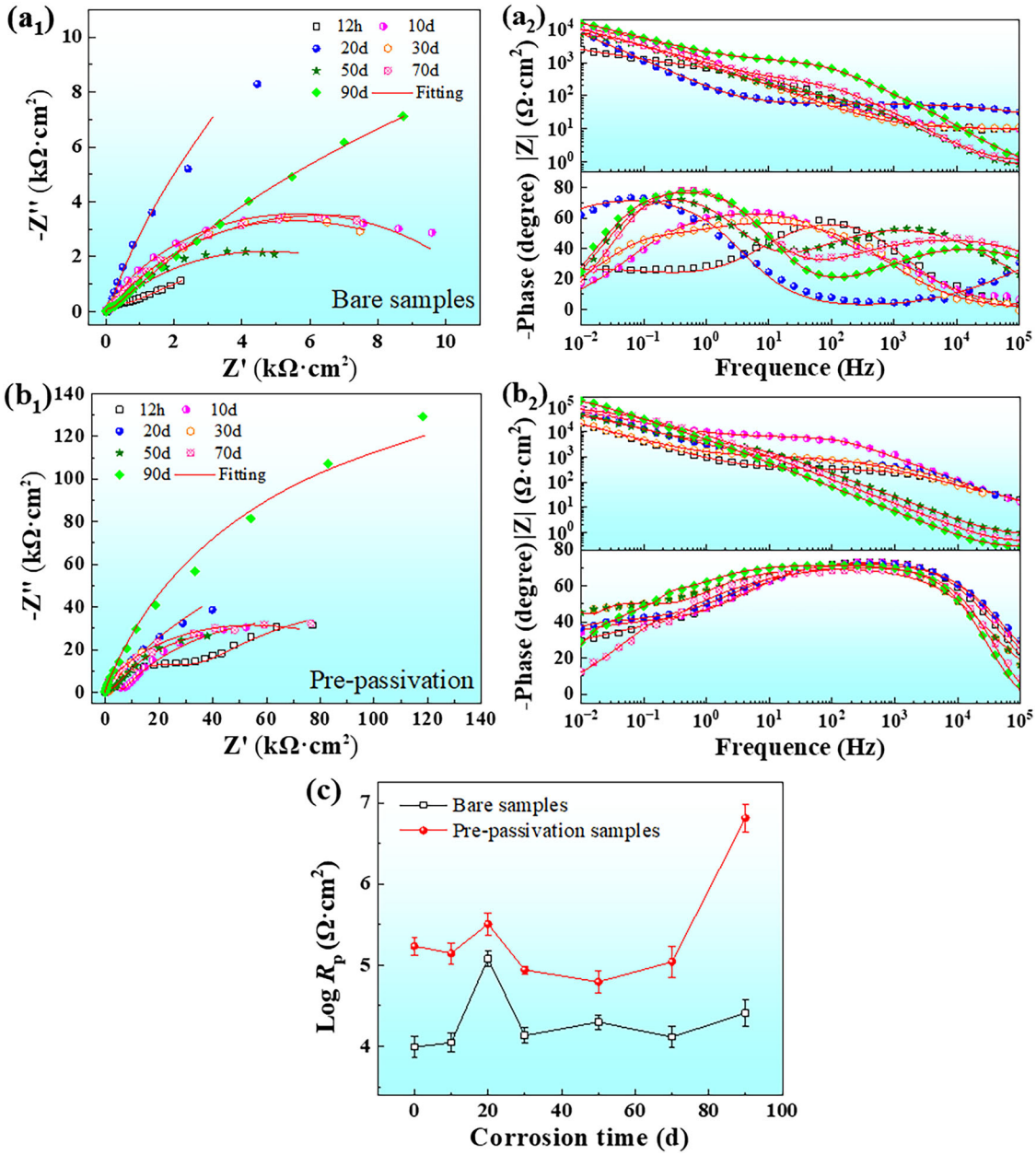

Fig. 6 | Electrochemical impedance spectra during 90 days of corrosion. a Bare copper samples; **b** pre-passivation samples under the optimal process; **c** variation curves of polarization resistance (R_p) with corrosion time.

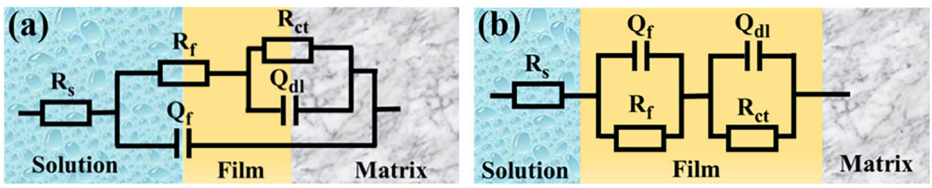

Fig. 7 | Equivalent electrical circuits used for fitting EIS spectra. a Bare samples; **b** pre-passivation samples.

shown in Fig. 9e, indicating that BTA has two states in the passivation film. A large number of studies have confirmed that Cu alloys can not only form complex Cu(I)-BTA in solutions containing BTA, but also BTA molecules can be directly adsorbed on the Cu surface[82]. In the C 1 s spectrum shown in Fig. 9f, C-O/C-N from BTA and C = O/O-C = O from SSA were detected, which verified again that the above two substances were involved in the formation of passivation film.

To further analyze composition distribution, time-of-flight secondary ion mass spectrometry (TOF-SIMS) depth profiling was performed on the passivation film formed under the optimal process, as shown in Fig. 10. Obvious delamination of passivation film components is observed; the outer layer is rich in BTA molecules, while the inner layer is dominated by Cu oxides and Cu(I)-BTA complexes. Yang et al.[24] also found that Cu has a similar structure in solution containing BTA and H_2O_2, which is attributed

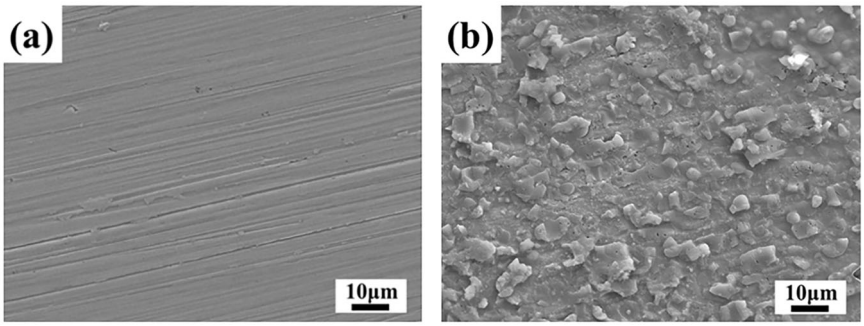

Fig. 8 | SEM surface morphology. a Bare copper sample; **b** pre-passivation sample.

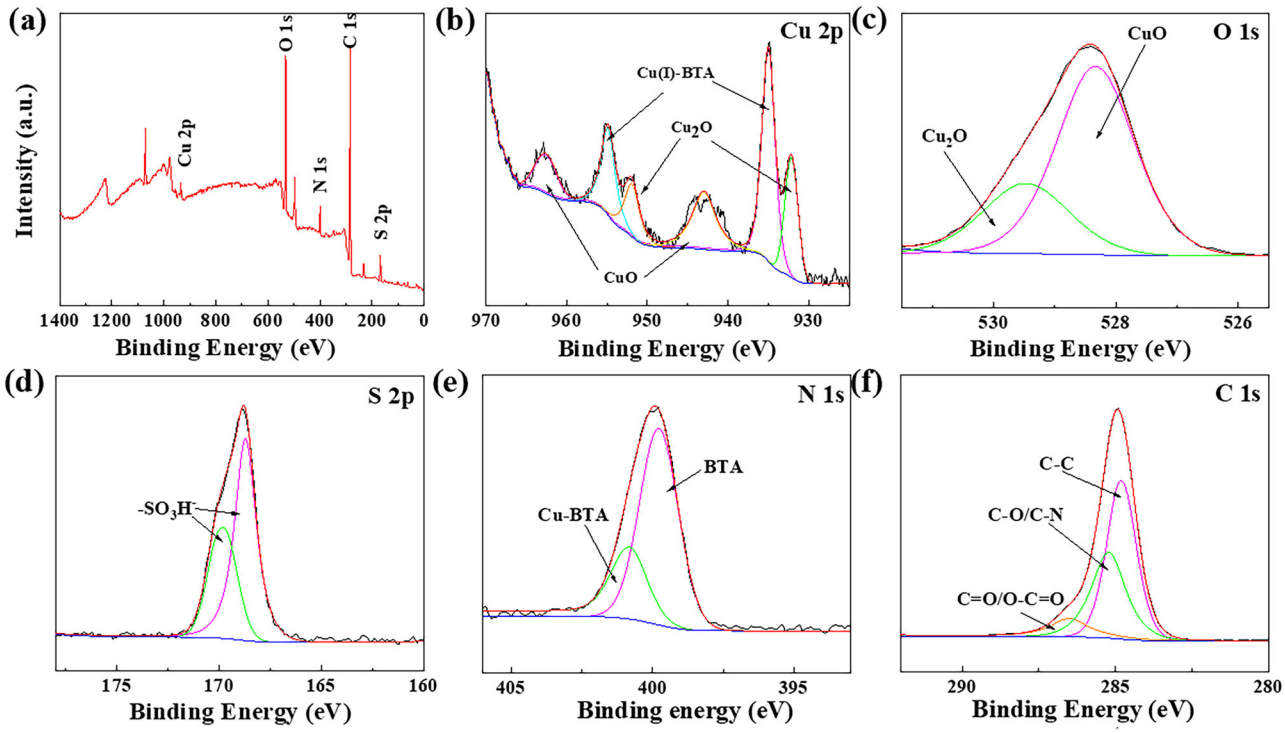

Fig. 9 | XPS analysis of organic passivation film formed under the optimal process. a XPS survey spectra; **b** Cu 2p; **c** O 1 s; **d** S 2p; **e** N 1 s; **f** C 1 s.

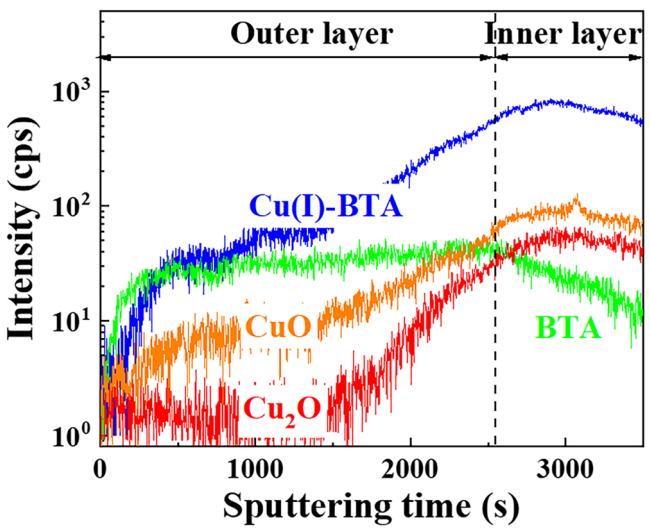

Fig. 10 | TOF-SIMS ion depth profiles for the organic passivation film formed under the optimal process.

to the following process: dissolution and oxidation of the matrix, adsorption of BTA, self-stabilization of the adsorbed film, and filling of the passivation film with oxide particles. There is no obvious interface between Cu oxide and Cu(I)-BTA complex. Chadwick and Hashemi[35] showed that the Cu(I)-BTA complex is unstable in corrosive environments, whether it is adsorbed on the Cu surface or synthesized as a crystal. Therefore, the outer BTA layer is beneficial to improve the stability of the inner Cu(I)-BTA complex.

Figure 11 shows the cross-sectional TEM images, corresponding energy-dispersive X-ray spectrometry (EDS) analysis, and elected area electron diffraction (SAED) patterns of the passivation film formed under the optimal process. Due to the high energy in the process of ion thinning, the passivation film and substrate are seriously damaged, and a large number of holes appear, as shown in Fig. 11a. The thickness of the passivation film is ~6 μm, SAED results of different regions show that the passivation film has amorphous structure[35,83], as shown in Fig. 11b, c. Due to the absence of crystal defects such as grain boundary, the amorphous structure of the passivation film has better corrosion resistance[14]. The passivation film is tightly bonded with the substrate, and no microcracks were observed at the interface. EDS analysis results show that the content of C in the passivation film gradually increased from inside to outside, while the content of Cu showed the opposite trend, as shown in Fig. 11d. The changes of C and Cu contents indicates that the contents of BTA and Cu containing products

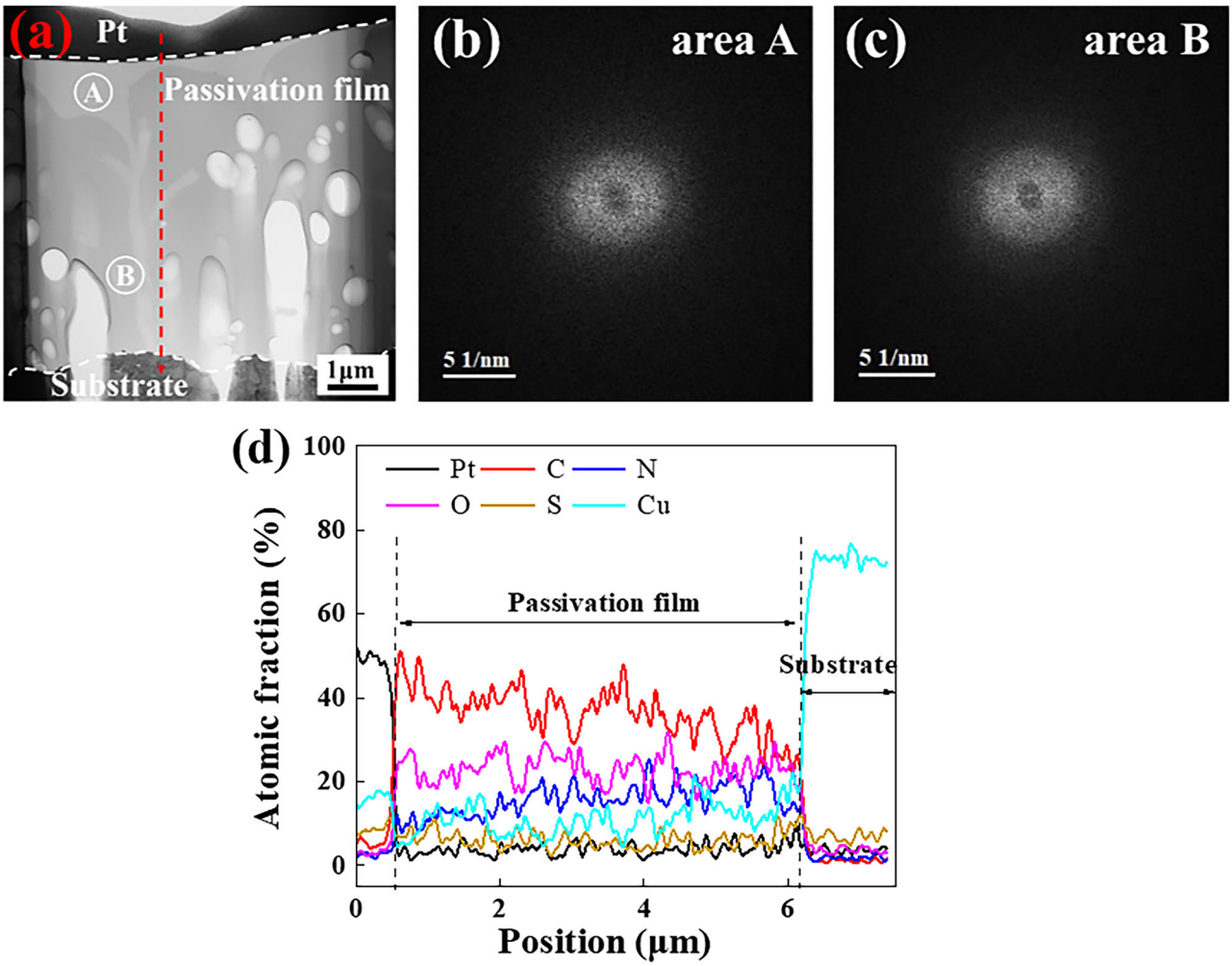

Fig. 11 | TEM characterization of the organic passivation film formed under the optimal process. a The cross-sectional image; **b**, **c** the corresponding selected area diffraction patterns; **d** the corresponding EDS analysis.

decreased and increased from outside to inside, respectively, which is consistent with the composition analysis of the passivation film in Fig. 10. Combined with the electrochemical measurements and characterization results, it was found that the thick amorphous passivation film formed under the optimal process had excellent corrosion resistance, which provided guidance for the further exploration of an effective B30 rapid pre-passivation treatment.

Effective pre-passivation treatment of B30 alloy and corrosion tests

Compared with pure copper, B30 alloy contains about 30% Ni and 0.7% Fe, so promoting the co-deposition of Ni and Fe products to form passivation film is the key to the transformation from pure copper to B30 alloy pre-passivation treatment process. Figure 12a shows the potentiodynamic polarization curve measurements of B30 alloy pre-passivation solution with different composition in 30°C, and the fitted electrochemical parameters are listed in Table 3. Basic solution (BS) is a solution for removing SSA based on the optimal pure copper pre-passivation solution. Its composition is as follows: BTA concentration of 14-16 g/L, H_2O_2 concentration of 10-11 ml/L, SDS concentration of 0.5 g/L. The results show that the pre-passivation B30 alloy exhibits the same anodic characteristics as the bare sample in base solution, indicating that no effective passivation film is formed on the substrate surface. After adding 2 g/L SSA to the base solution, the anodic polarization curve of the pre-passivation B30 alloy moves in the direction of the decrease of current density, and an obvious passivation zone appears, which is attributed to the acid environment accelerating the dissolution of the matrix and promoting the formation of the passivation film[60,84]. In contrast, after adding 3 g/L H_3PO_4 to the basic solution, the corrosion resistance of pre-passivation B30 alloy was significantly improved, showing better passivation performance. E_{pit} increased to 0.39 V (vs SCE) and i_p decreased by 15 times, as shown in Table 3. Therefore, it is feasible to use H_3PO_4 instead of SSA in the passivation solution to improve the corrosion resistance of passivation film. Figure 12b shows the potentiodynamic polarization curves of B30 alloy in passivation solutions with different H_3PO_4 concentration, and the fitted electrochemical parameters are listed in Table 3. E_{pit} first increased and then decreased with the increase of H_3PO_4 concentration, reaching the maximum at 3 g/L. i_p first decreased and then increased with the increase of H_3PO_4 concentration, reaching the minimum at 3 g/L, as shown in Table 3, indicating that 3 g/L H_3PO_4 is the best choice. Furthermore, Fig. 12c shows the effect of temperature on the corrosion resistance of passivation film. After pre-passivation treatment at 30°C, B30 alloy shows good passivation performance and high E_{pit}, as shown in Table 3. According to the 'Dissolution-Ionization-Diffusion-Deposition' model[85], B30 alloy dissolves faster than pure copper and produces more metal ions. Reducing the pre-passivation temperature slightly is beneficial to improve the stability of H_2O_2, and its effect is more significant than reducing matrix dissolution rate. Based on the above analysis, the pre-passivation process suitable for B30 alloy is obtained: BTA concentration of 14–16 g/L, H_3PO_4 concentration of 3 g/L, H_2O_2 concentration of 10-11 ml/L, SDS concentration of 0.5 g/L and temperature of 30 °C.

Figure 13 presents the EIS spectra of B30 bare samples and pre-passivation samples during 30 days of static immersion. With the extension

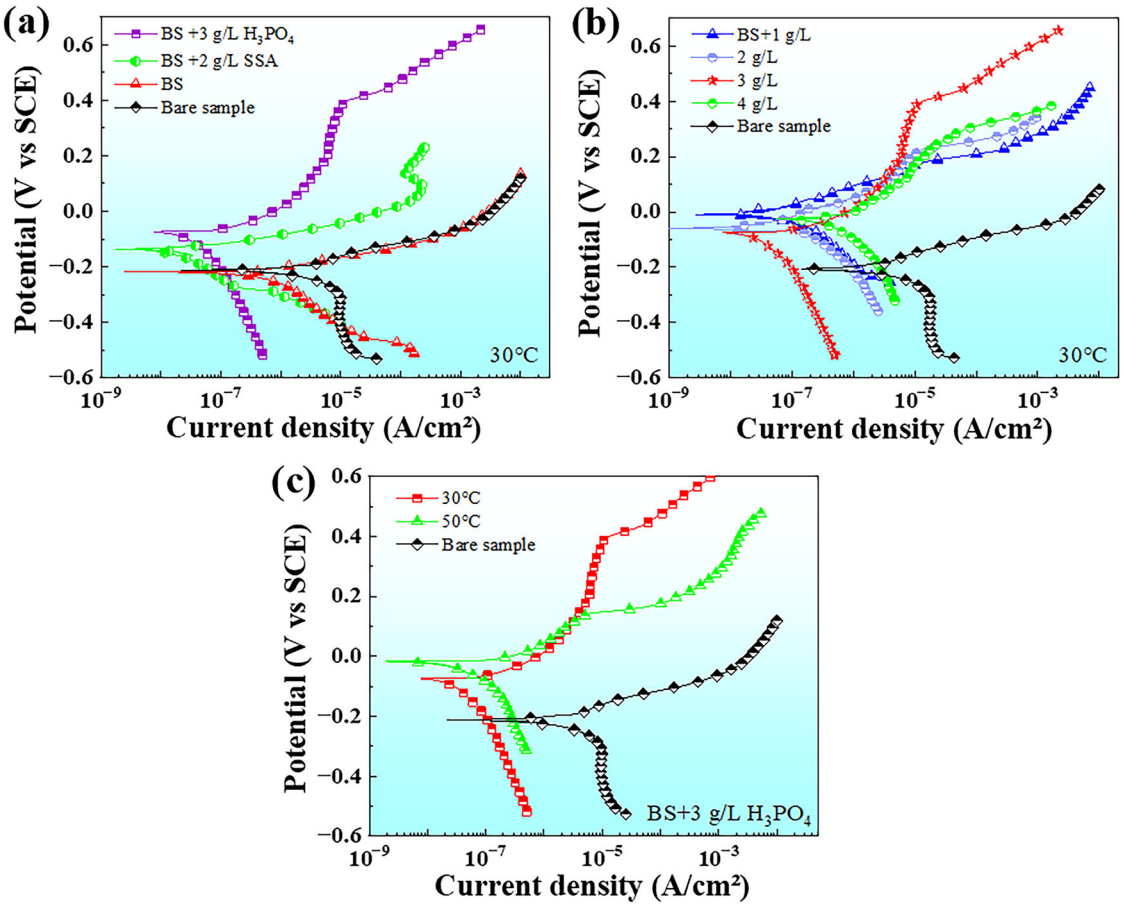

Fig. 12 | Potentiodynamic polarization curves of the pre-passivation samples formed at different parameters. a Different acid solutions, **b** different concentration of H_3PO_4, **c** different passivation temperature.

of corrosion time, the radius of the capacitance arc of the B30 bare sample increases, indicating that a protective film is gradually formed on the bare sample, as shown in Fig. 13(a1). In the Bode plot shown in Fig. 13(a2), the low-frequency |Z| values and maximum phase angles increase with the extension of corrosion time, which indicates that the corrosion product film is gradually compact and corrosion resistant. In contrast, the radius of the capacitance arc of pre-passivation samples suddenly increased after 10 days of corrosion, and then remained stable, as shown in Fig. 13(b1). In the Bode plot shown in Fig. 13(b2), the low-frequency |Z| values and maximum phase angles do not change significantly with the extension of corrosion time, indicating that the passivation film has good stability. The equivalent circuit shown in Fig. 7 is used to fit the EIS parameters of the B30 bare samples and pre-passivation samples, and the fitted electrochemical parameters are listed in Table S4. According to the fitted electrochemical parameters, n_f, R_f and R_{ct} values of the pre-passivation samples are much greater than those of the bare samples, indicating a more compact structure of the pre-passivation film and greater resistance to further corrosion of the alloy. The change of R_p value of bare sample and pre-passivation sample with corrosion time is displayed in Fig. 13c. The R_p value of bare samples increased rapidly within 20 days of corrosion, and then increased slowly, indicating that the protective corrosion film was gradually formed, and the 'infancy' was 20 days. In contrast, the R_p value of the pre-passivation sample is relatively stable during the whole immersion period. Compared with the bare sample, the pre-passivation samples showed a higher R_p value, especially in the 'infancy', which increased by 1.5-2 orders of magnitude.

Figure 14 shows the EIS spectra of B30 bare samples and pre-passivation samples during 30 days flow-accelerated corrosion. For B30 bare sample, the radius of the capacitance arc increases with corrosion time, as shown in Fig. 14(a1). Compared with bare sample under static immersion (Fig. 13(a1)), the fluid accelerated the formation of protective corrosion film[14], and showed a larger radius of the capacitance arc after 10 days of corrosion. In the Bode plots (Fig. 14(a2)), the low-frequency |Z| values and maximum phase angles increase with the extension of corrosion time, especially within 10 days, which indicates that a protective film is gradually formed on the B30 alloy bare samples after its 'infancy' (10 days). For pre-passivation samples shown in Fig. 14(b1), the radius of the capacitance arc decreases with the corrosion time, indicating that the passivation film is damaged during the 30 days flow accelerated corrosion. In the Bode plot shown in Fig. 14(b2), the low-frequency impedance value decreases and maximum phase angles continuously fluctuating with corrosion time. According to the fitted electrochemical parameters shown in Table S4, n_f values of the pre-passivation film under flow accelerated corrosion is lower than those under static immersion, indicating a severe damage for the pre-passivation film in the fluid environment. However, n_f, R_f, and R_{ct} values of the pre-passivation film are higher than those of bare samples. Figure 14c shows the evolution of R_p values for bare sample and pre-passivation sample during 30 days flow-accelerated corrosion. Within 20 days of corrosion, the R_p value of bare sample increased rapidly, indicating that the 'infancy' was 20 days. Although the R_p value of the pre-passivation sample decreased continuously during the whole immersion period, it was still higher than that of the bare samples. Especially in 'infancy', the R_p value of pre-passivation samples increased by 0.5–2 orders of magnitude. The above EIS analysis results show that the pre-passivation treatment can effectively help B30 alloy survive its 'infancy' during shutdown and operation in an aggressive deep-sea environment.

Figure 15 shows the surface morphology of the bare samples and pre-passivation samples during 30 days of static immersion. Before the corrosion test, there were obvious grinding marks on the surface of the B30 bare

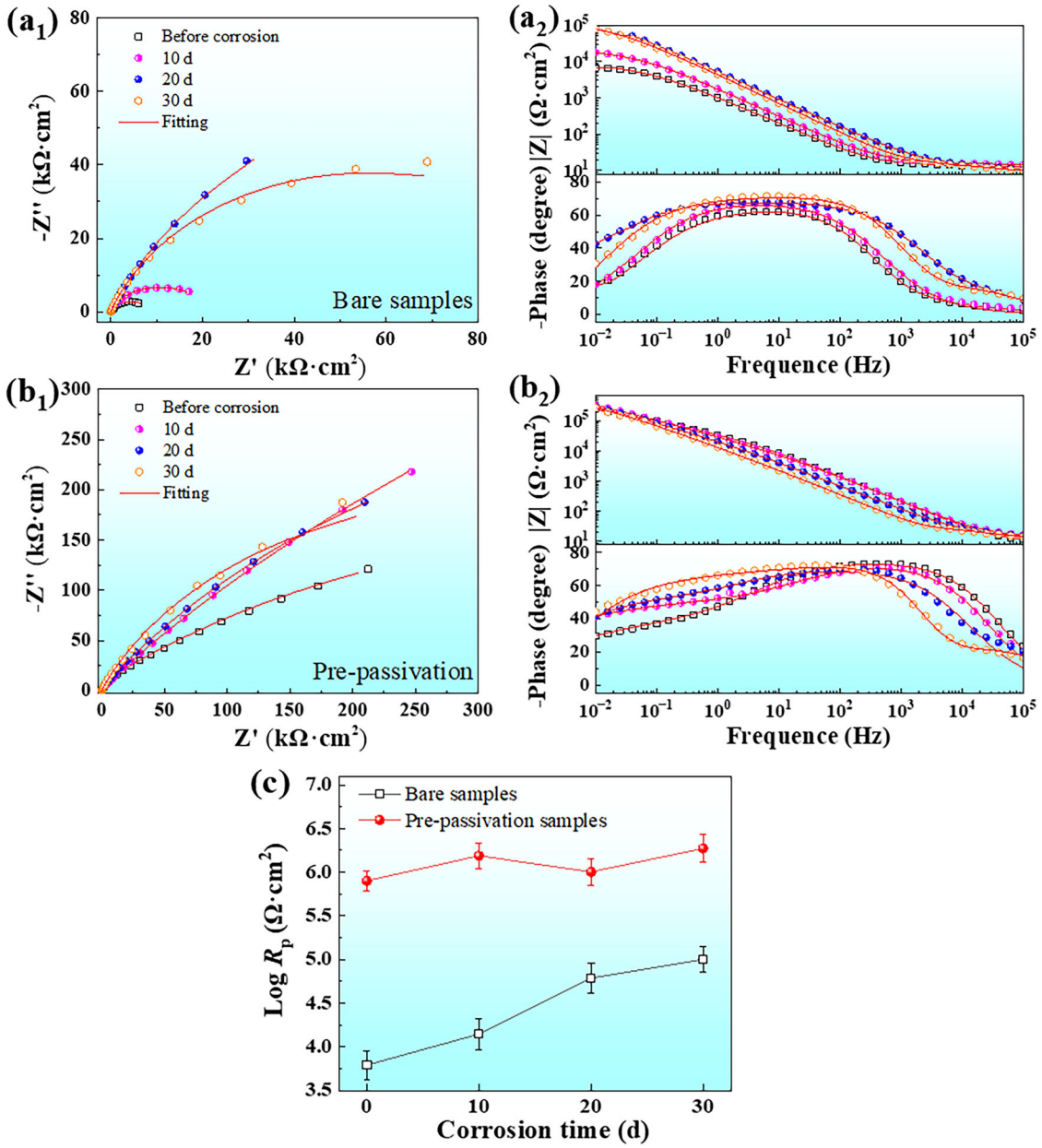

Fig. 13 | Electrochemical impedance spectra during 30 days of static immersion. a B30 bare sample; **b** pre-passivation samples; **c** variation curves of polarization resistance (R_p) with corrosion time.

sample. With the extension of corrosion time, the grinding marks gradually disappear and the surface becomes more uniform, which may be attributed to the formation of corrosion film. After pre-passivation treatment, an organic passivation film is formed on the surface of B30 alloy, and there are some micropores on the surface of passivation film, as shown in Fig. 15e. Liao et al.[45] also found that similar micropores exist when Cu-0.25Se-0.25Te alloy is immersed in 3.5 wt% NaCl solution containing BTA. With the extension of corrosion time, obvious cracks appeared on the surface of passivation film, which may be attributed to the combination of micropores. Figure 16 shows the surface morphology of bare samples and pre-passivation samples during 30 days of flow-accelerated corrosion. For B30 bare samples, corrosion film gradually formed on the surface of the substrate with the extension of corrosion time. Compared with static immersion, slight grinding marks were observed during flow accelerate corrosion,

Table 3 | Electrochemical parameters obtained by potentiodynamic polarization curves in Fig. 12

	Temperature	E_{pit} (V vs SCE)	i_p (μA/cm²)
Bare sample	30°C	No passivation	
Basic solution (BS)		No passivation	
BS + 1 g/L H_3PO_4		No passivation	
BS + 2 g/L H_3PO_4		0.21 ± 0.08	7.42 ± 0.79
BS + 3 g/L H_3PO_4		0.39 ± 0.11	6.82 ± 0.12
BS + 4 g/L H_3PO_4		0.24 ± 0.09	12.65 ± 1.38
BS + 2 g/L SSA		0.14 ± 0.03	97.31 ± 8.27
BS + 3 g/L H_3PO_4	50°C	0.14 ± 0.07	3.70 ± 0.82

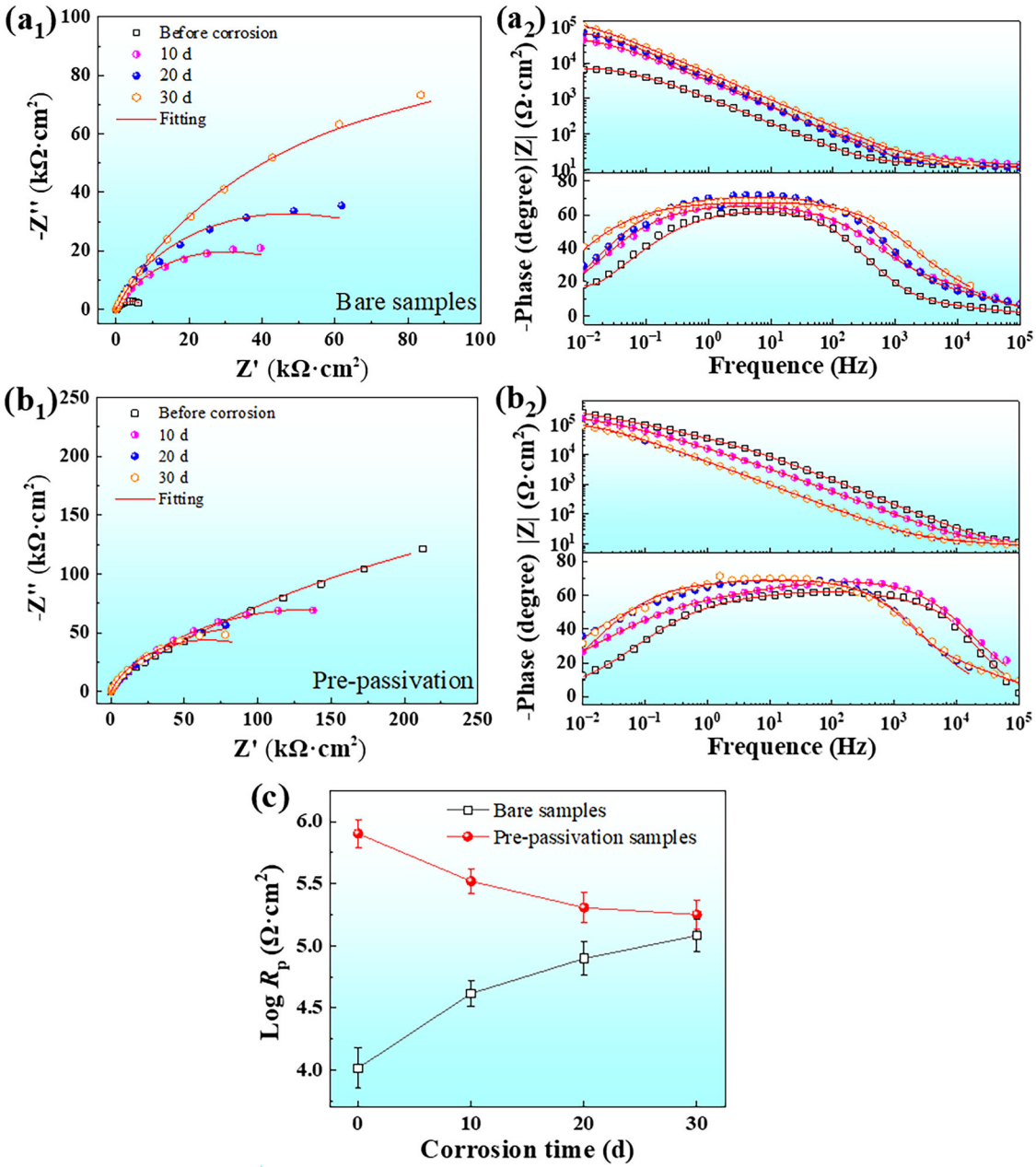

Fig. 14 | Electrochemical impedance spectra during 30 days of flow-accelerated corrosion. a B30 bare sample; **b** pre-passivation samples; **c** variation curves of polarization resistance (R_p) with corrosion time.

indicating the formation of a thicker corrosion film. For the pre-passivation samples, cracks also appeared on the surface of the passivation film during 30 days of flow-accelerated corrosion.

Figure 17a presents the cross-sectional morphology of the organic passivation film before the corrosion test. Some micropores were observed in the outer layer of the passivation film, which was consistent with the SEM surface morphology shown in Fig. 15e. However, the inner layer of the organic passivation film is relatively dense and tightly bonded to the B30 alloy substrate, and no micropores or cracks are observed at the interface. EDS analysis results show that the passivation film contained a large amount of C, a small amount of Cu, Ni, O, and N, indicating that Cu and Ni are involved in the formation of the passivation film. After 30 days of static immersion, a double-layer structure corrosion film is formed on the surface of the B30 alloy substrate, as shown in Fig. 17b. The outer layer of the corrosion film is the original passivation film, which is rich in C. The inner layer of the corrosion film is a dense regenerated film, which is rich in Cu, Ni, and O. It can be seen that the organic passivation film is only slightly damaged during 30 days of static immersion, which ensures that the B30 alloy can safely survive the 'infancy' and form a dense regenerative film. Previous studies have found that dense regenerated film can reduce the corrosion rate of heat-transfer tubes in the subsequent service process[14]. The formation of regenerated film is consistent with the increase of R_p with the extension of corrosion time, as shown in Fig. 13c. After 30 days of flow-accelerated corrosion, a similar double-layer structure corrosion film was also observed in Fig. 17c, with the outer layer being the original organic passivation film, and the inner layer being the dense regenerated film. Combined with electrochemical tests, it can be seen that the combination of organic passivation film and regenerated oxide film plays a key role in reducing the corrosion rate of B30 alloy.

The microstructure of the passivation film was further analyzed by TEM before and after corrosion tests. Figure 18 shows the TEM cross-sectional images, the corresponding EDS analysis, and SAED patterns of the

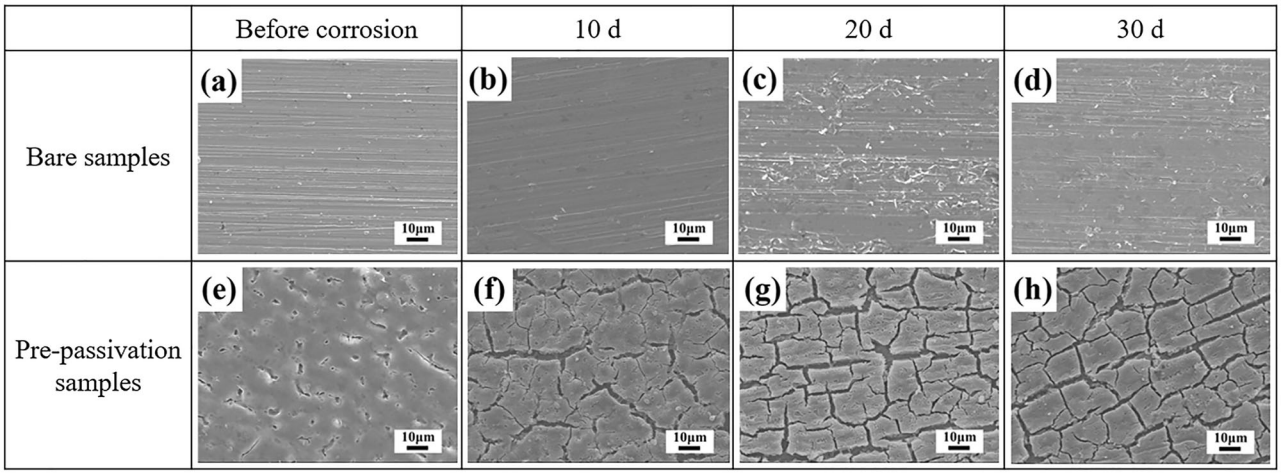

Fig. 15 | Surface corrosion morphologies of the B30 bare samples and pre-passivation samples during 30 days of static immersion.

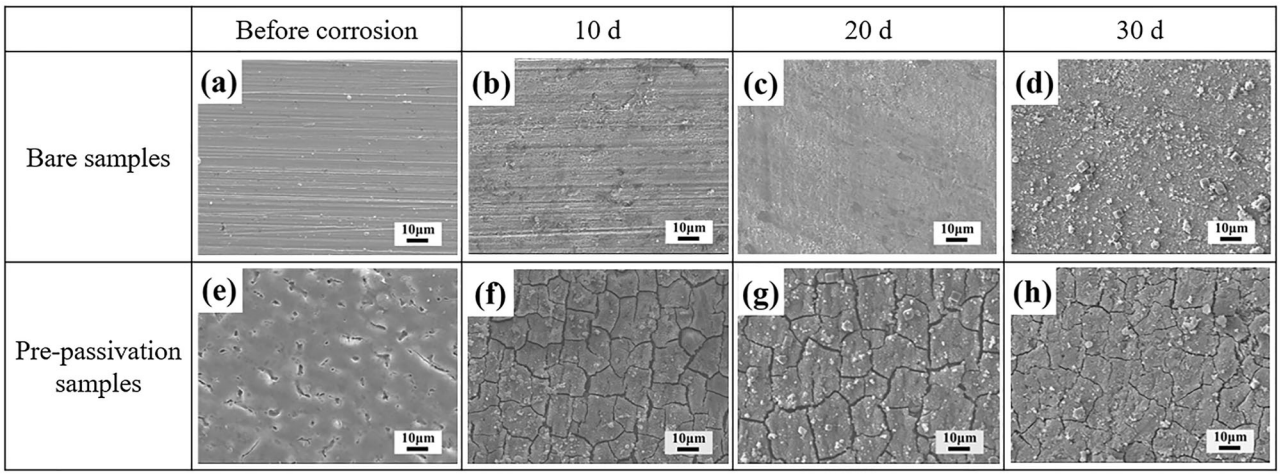

Fig. 16 | Surface corrosion morphologies of the B30 bare samples and pre-passivation samples during 30 days of flow accelerated corrosion.

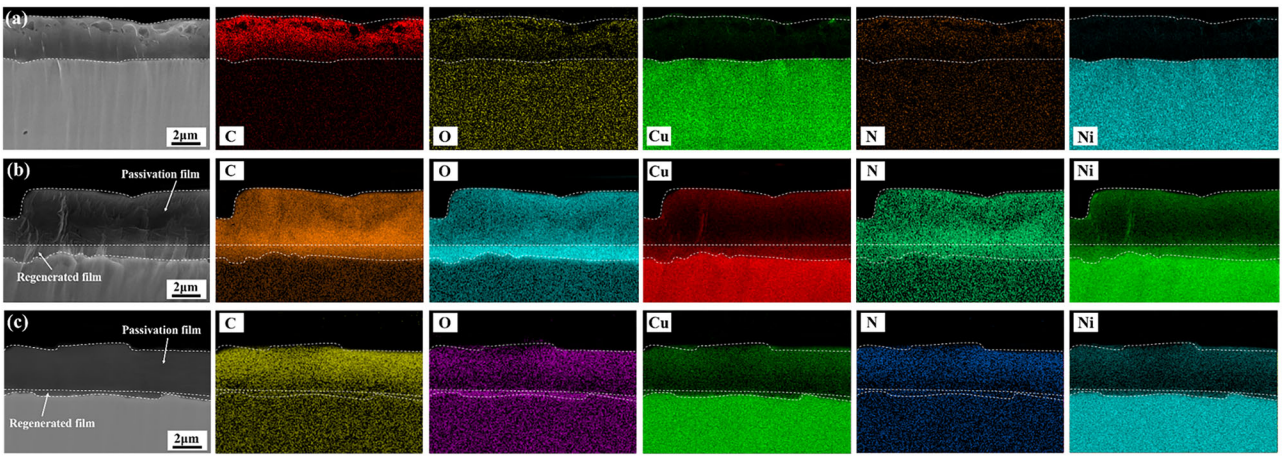

Fig. 17 | Cross-sectional corrosion morphologies of the pre-passivation samples. a Before corrosion; **b** after 30 days of static immersion; **c** after 30 days of flow accelerated corrosion.

passivation film before the corrosion tests. A 4 μm passivation film is formed on the substrate surface after pre-passivation treatment, and some holes appear in the outer layer of passivation film, as shown in Fig. 18a. The inner layer of the passivation film is uniform and compact, and tightly bonded with the substrate. The SAED result shown in Fig. 18b indicate that the passivation film has an amorphous structure. Finsgar et al. also proved the amorphous structure of BTA, Cu(I)-BTA, Ni(II)-BTA[35]. The line-scan EDS results in Fig. 18c indicate that C is mainly enriched in the whole film, and Cu, Ni, and Fe participate in the formation of passivation film. Moreover, due to the addition of low-concentration H_3PO_4, a small amount of P was

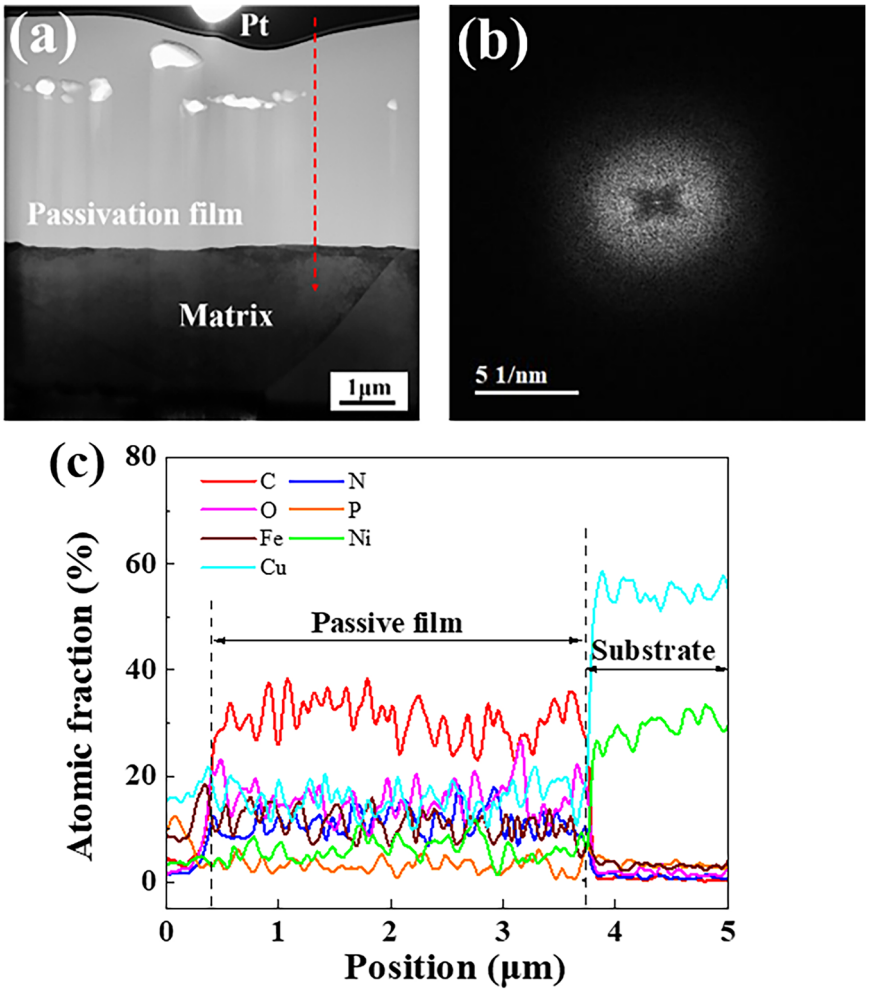

Fig. 18 | TEM characterization of the organic passivation film before corrosion tests. a The cross-sectional images; **b** the corresponding selected area diffraction pattern; **c** the corresponding EDS analysis.

also detected in the passivation film. Figure 19 shows the cross-sectional TEM images, corresponding EDS analysis, and SAED patterns of the organic passivation film after 30 days of static immersion. The organic passivation film has low mechanical strength and is easily damaged in the process of ion thinning. Figure 19a shows that the organic passivation film near the regenerated film was seriously damaged during sample preparation. After 30 days of static immersion, the organic passivation film was slightly damaged, and the thickness was basically unchanged. SAED analysis of region A indicates that the organic passivation film has an amorphous structure, as shown in Fig. 19d. Furthermore, a dense regenerated film was formed on the substrate surface, as shown in Fig. 19c. SAED analysis of region B indicates that the regenerated film had amorphous structure and contained some nanocrystalline Cu_2O. The line-scan EDS results in Fig. 19f indicate that the regenerated film is composed of Cu and Ni oxides. Ma et al. found that NiO in the corrosion products of Cu-Ni alloy was amorphous structure[6]. Our previous research also found that the amorphous NiO based regenerated film has good corrosion resistance[14]. During sample preparation, there was still obvious damage between the organic passivation film and the regenerated film, as shown in Fig. 20a. After 30 days of flow accelerated corrosion, the thickness of organic passivation film decreased significantly due to the mechanical effect of the fluid. SAED analysis of region A indicates that the organic passivation film also has amorphous structure, as shown in Fig. 20d. Moreover, the regenerated film is formed beneath the organic passivation film, as shown in Fig. 20c. EDS analysis results are shown in Fig. 20g, indicating that the regenerated film was composed of Ni and Cu oxides, in which Ni oxide was the main component. SAED results of regions B and C indicate that the regenerated film has an amorphous structure and contains some nanocrystalline Cu_2O, as shown in Fig. 20e, f. It can be seen that the substrate protected by an organic passivation film forms an amorphous structure film after 'infancy', which is crucial for prolonging the service life of heat-transfer tubes. A large number of studies have confirmed that amorphous passivation films and coatings have excellent corrosion resistance in static and dynamic corrosive environments[14,86–88].

Figure 21 shows the TOF-SIMS results of bare and pre-passivation B30 alloy samples after 30 days of corrosion test. After 30 days of static immersion (Fig. 21a), corrosion films mainly composed of NiO, CuO, γ-FeOOH and a small amount of Cu_2O were formed on the bare sample of B30 alloy. After 30 days of flow accelerated corrosion (Fig. 21b), the thickness of corrosion film on the bare sample of B30 alloy increased significantly, which can also be observed from the SEM corrosion morphology shown in Fig. 16d. The corrosion film has a multi-layer structure, the outer layer is mainly composed of γ-FeOOH, and the inner layer is mainly composed of Cu and Ni oxides. In addition, loose $Cu_2(OH)_3Cl$ was also observed in the corrosion film. This kind of multi-layer structure film has been found in the research of other scientists[6]. For the pre-passivation samples (Fig. 21c), the passivation film is composed of Cu(I)-BTA, Ni(II)-BTA, NiO, Cu_2O, BTA, $FePO_4$ and $Ni_3(PO4)_2$, indicating that both Cu, Ni and Fe are involved in the formation of the passivation film. Furthermore, H_3PO_4 also participated in the deposition of the film, forming $FePO_4$ and $Ni_3(PO4)_2$, which is consistent with TEM analysis shown in Fig. 18c. Guo et al. have confirmed that $FePO_4$ is closely and evenly distributed on the alloy surface as a barrier layer for the alloy matrix[71]. It can be seen that $FePO_4$ is conducive to improving the compactness of the pre-passivation film, which

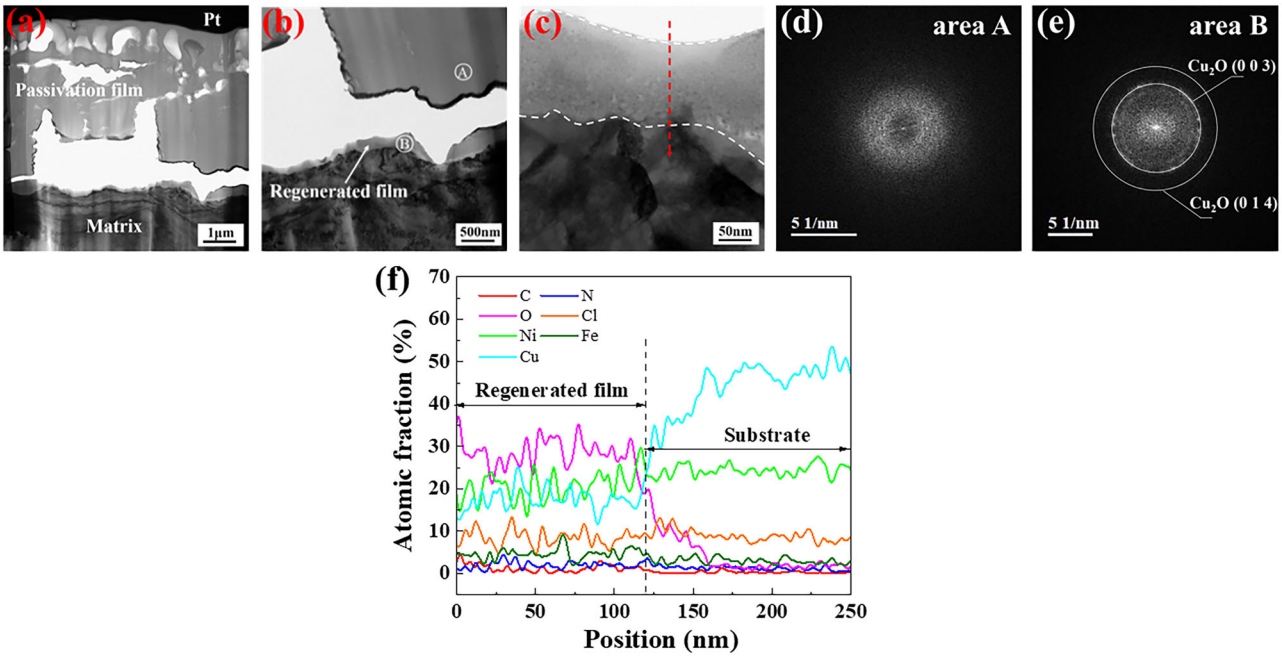

Fig. 19 | TEM characterization of the corrosion film after 30 days of static immersion. a–c The cross-sectional images; **d**, **e** the corresponding selected area diffraction patterns; **f** the corresponding EDS analysis.

Fig. 20 | TEM characterization of the corrosion film after 30 days of flow accelerated corrosion. a–c The cross-sectional images; **d–f** the corresponding selected area diffraction patterns; **g** the corresponding EDS analysis.

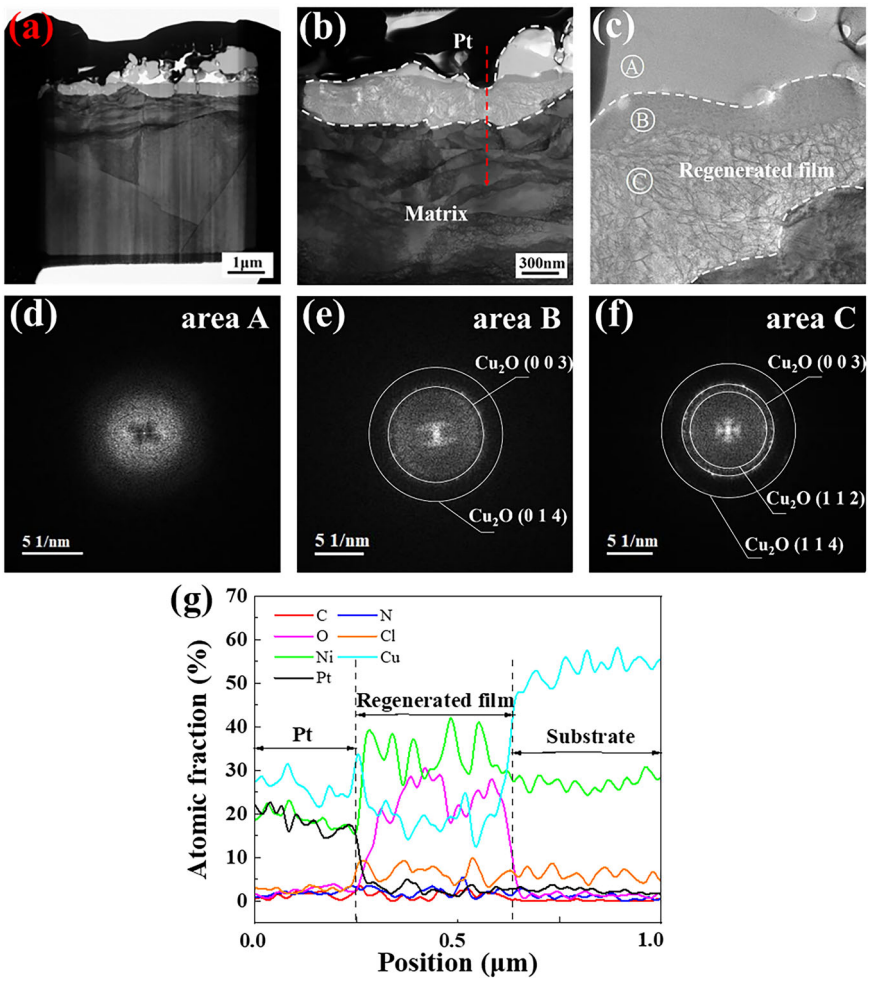

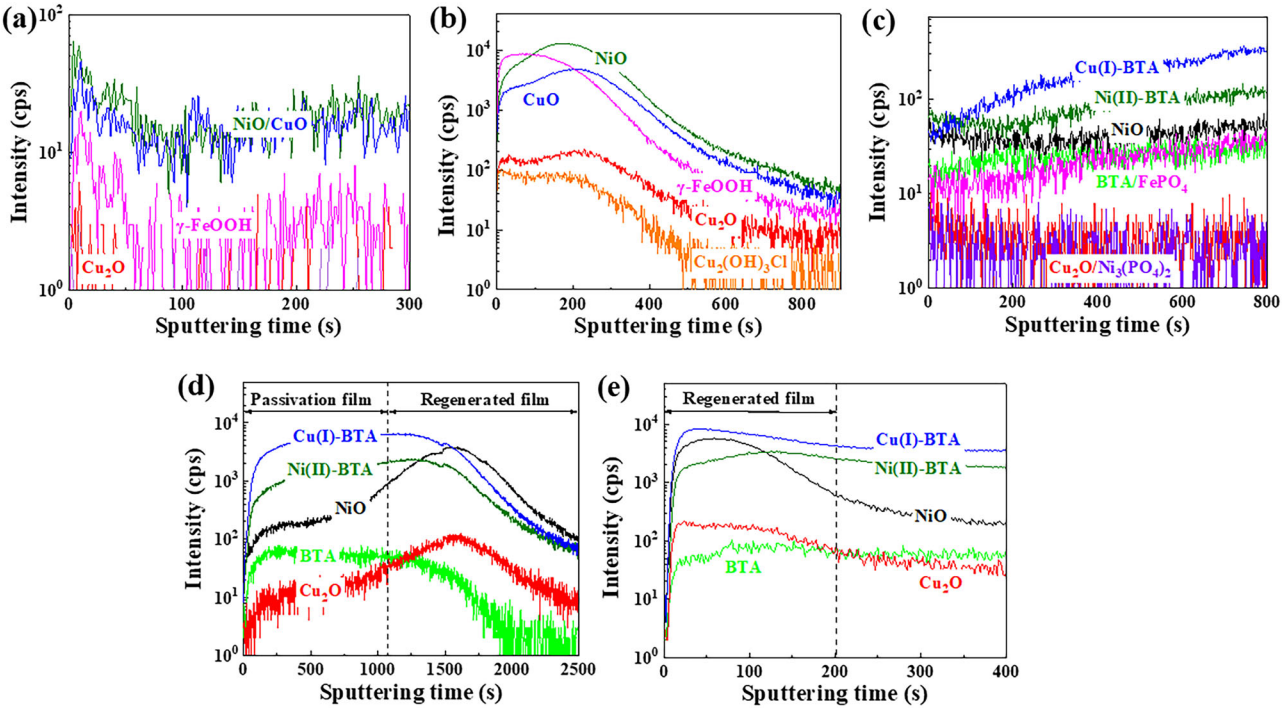

Fig. 21 | TOF-SIMS ion depth profiles analysis. a B30 bare samples after 30 days of static immersion; **b** bare samples after 30 days of flow accelerated corrosion; **c** pre-passivation samples before corrosion; **d** pre-passivation samples after 30 days of static immersion; **e** pre-passivation samples after 30 days of flow accelerated corrosion.

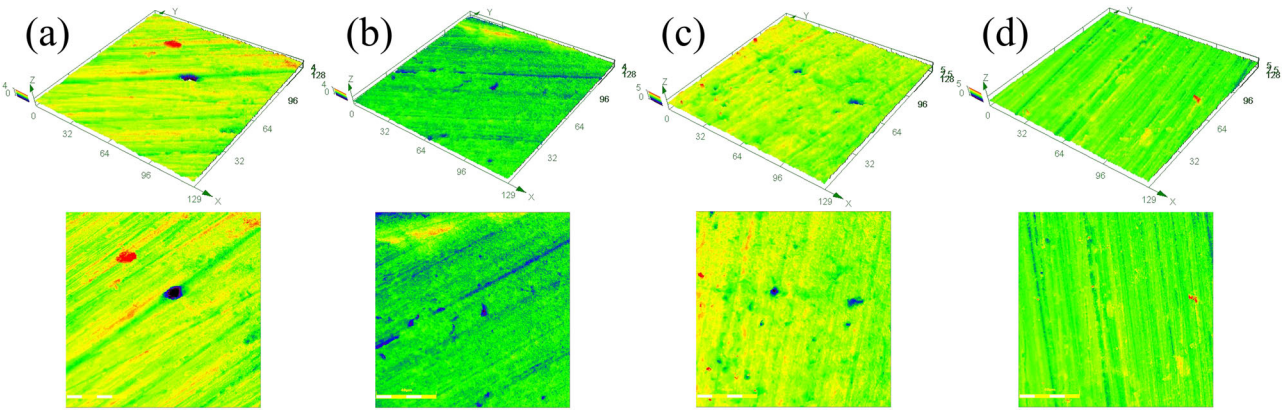

Fig. 22 | 3D corrosion morphology after removal of corrosion products. a Bare samples after static immersion; **b** bare samples after flow accelerated corrosion; **c** pre-passivation samples after static immersion; **d** pre-passivation samples after flow accelerated corrosion.

is consistent with the electrochemical test results shown in Fig. 12a. After 30 days of static immersion (Fig. 21d), a bilayer structure film was detected. The outer layer is an organic passivation film, which exhibits a composition similar to that shown in Fig. 21c. The inner layer is a regenerated film mainly composed of NiO and Cu_2O, which is consistent with the SAED and EDS analysis shown in Fig. 19e, f. After 30 days of flow accelerated corrosion (Fig. 21e), Cu(I)-BTA, Ni(II)-BTA, NiO, Cu_2O, BTA were detected in the corrosion film. Different from Fig. 21d, no delamination of corrosion film is observed. According to the enrichment of NiO and Cu_2O in Fig.21e and the TEM analysis in Fig. 20, it can be judged that a regenerated film was formed beneath the organic passivation film.

The 3D confocal laser scanning microscopy was used to observe the 3D corrosion morphology of the substrate after removal of corrosion products. After 30 days of static immersion, localized corrosion pits appear on the surface of the B30 bare sample, as shown in Fig. 22a. For the pre-passivation samples shown in Fig. 22b, small localized corrosion pits were also observed on the substrate. The cumulative probability of the Pit_{max} depth (Fig. 23) shows that the pits formed on the surface of the pre-passivation samples were shallow. After 30 days of flow accelerated corrosion, some small localized corrosion pits appeared on the surface of B30 bare sample, as shown in Fig. 22c. Compared with the static immersion, the localized corrosion pits formed on the bare samples in fluid environment are shallower, as shown in Fig. 23. Zhao et al.[88] found that the geometry of corrosion pits in fluid environment changed from bullet shaped to shallow disc-shaped. For the pre-passivation samples shown in Fig. 22d, no localized corrosion pits were observed, indicating that the B30 alloy substrate beneath the organic passivation film experienced uniform corrosion in the fluid environment. The above analysis shows that the organic passivation film can effectively isolate the corrosive medium from the alloy substrate, thereby inhibiting the localized corrosion of the alloy substrate and reducing the risk of perforation in heat-transfer tubes.

According to the above results of the electrochemical test and characterization analysis for pure copper and B30 alloy, the following conclusions can be drawn: Firstly, for pure copper, BTA concentration is the most

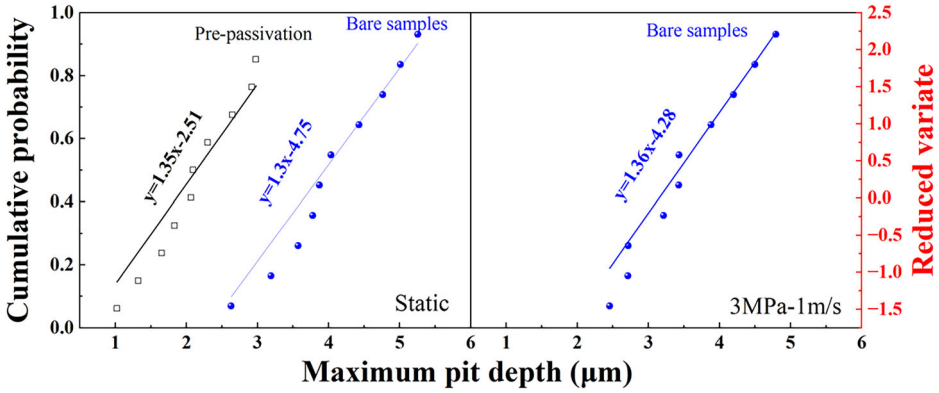

Fig. 23 | Cumulative probability and reduced variant of maximum pit depth of bare samples and pre-passivation samples after 30 d of corrosion tests.

Table 4 | The upper and lower limits of the independent variables

Independent variable	Lower limit	Upper limit
BTA (g/L)	4	20
Sulfosalicylic acid (g/L)	1	5
H_2O_2 (ml/L)	10	30
Temperature (°C)	25	50

important process parameter, which has interactions with other parameters. The degree of influence on corrosion resistance of organic passivation film decreased in the following order: BTA > BTA × SSA > H_2O_2 > SSA > Temperature > BTA × Temperature > BTA × H_2O_2. SSA and H_2O_2 both accelerate the dissolution of pure copper and forms sufficient metal ions, in this case, the increase of BTA concentration promotes the formation kinetics of passivation film, thus providing better corrosion resistance. Although temperature can accelerate the formation rate of pre-passivation film, it reduces the stability of H_2O_2. Therefore, there is an optimal range for the interaction between temperature and BTA. Considering the single factors and their interactions, the optimal process for rapid pre-passivation of pure copper was predicted as follows: BTA concentration of 14-16 g/L, SSA concentration of 2-2.3 g/L, H_2O_2 concentration of 10-11 ml/L, SDS concentration of 0.5 g/L and temperature of 45–50°C. Secondly, for B30 alloy, the organic passivation film showed better corrosion resistance after the SSA was replaced by H_3PO_4 in the pre-passivation system. The pitting potential increased by 0.25 V, and the passive current density decreased by 15 times. The excellent passivation performance is attributed to the deposition of $FePO_4$ and $Ni_3(PO4)_2$, they not only serve as heterogeneous nucleation sites to accelerate the formation kinetics of pre-passivation films, but also act as fillers to improve the compactness of passivation films. The results showed that the BTA concentration of 14-16 g/L, H_3PO_4 concentration of 3 g/L, H_2O_2 concentration of 10-11 ml/L, SDS concentration of 0.5 g/L and temperature of 30°C was an improved pre-passivation process suitable for B30 alloy. Finally, the improved organic passivation film is helpful for B30 alloy to survive its 'infancy' safely, and ensure the formation of dense amorphous oxide film beneath the organic passivation film. There are no crystal defects, such as grain boundary, in the double-layer amorphous film, which makes it difficult for Cl^- to diffuse inward to the film/substrate interface, thus inhibiting the localized corrosion of the alloy substrate and reducing the risk of heat-transfer tube perforation. This pre-passivation treatment provides good protection for the subsequent service of the B30 heat-transfer tube and prolongs its service life in an aggressive deep-sea environment.

Methods

Materials

Commercial pure copper (99.90%) and B30 copper-nickel alloy were used as the experimental materials in this work, whose chemical composition was analyzed by ICP-OES (Optima 8300, Singapore). The composition (wt%) of B30 alloy was: Ni, 30.6%; Mn, 0.67%; Fe, 0.69%; Si, 0.01%; S, 0.006%; C, 0.052%; Cu, balance. Pure copper and B30 alloy plates were cut into specimens with a size of 10 mm × 10 mm × 3 mm for characterization and electrochemical testing. Before the test, all samples were wet ground to 2000 grit, rinsed with ethanol, and dried with cold air flow.

Design of the RSM

RSM experiment was designed by using Design-Expert 11 software to explore the optimal pre-passivation treatment process. BTA, SSA, H_2O_2, temperature were selected as independent variables, and the optimal range of each parameter was determined through literature research, as listed in Table 4. The accuracy of response surface is related to the number of test groups to some extent. If a small-scale or minimum scale experiment is designed to adapt to the modeling of a large number of variables, the resulting model usually does not have sufficient predictive accuracy[89]. Therefore, 53 groups of RSM experiments were designed to improve the accuracy of response surface, as shown in Table S1. Pre-passivation treatments were conducted according to conditions listed in Table S1. The pitting potential (E_{pit}) and passive current density (i_p) obtained from potentiodynamic polarization curve were used as response variables to analyze the corrosion resistance of BTA passivation film. Considering the influence of single factors and interaction, the optimal pre-passivation treatment process was predicted.

Pre-passivation treatment procedure

Before the pre-passivation treatment, the following pretreatment was conducted: Firstly, in order to remove the oil stain formed on the metal surface due to machining and improve the surface finish of the substrate, the samples were washed using a specific alkaline solution at 40–50 °C for 4 min. The concentrations of alkaline washing solution are as follows: Na_2CO_3 concentration of 50 g/L, NaOH concentration of 5 g/L, and Na_3PO_4 concentration of 50 g/L. Secondly, the samples were soaked in H_2SO_4 (10%) at 25 °C for 20 min to remove the oxide layer and improve the activity of the substrate surface, which is beneficial to improve the adhesion between the passivation film and the substrate. After the sample is rinsed with deionized water, conduct pre-passivation treatment for 30 min, the composition of pre-passivation treatment solution is shown in RSM table (Table S1). A magnetic stirring thermostatic water bath was used to maintain the temperature of the pre-passivation solution and accelerate the passivation process.

Corrosion tests of the pre-passivation film

The corrosion test of B30 alloy after the pre-passivation treatment was carried out to evaluate the corrosion resistance of the passivation film. The total corrosion test time was 30 days. Static immersion (temperature-pressure-flow rate: 25°C–0.1 MPa–0 m/s) and flow accelerated corrosion

Table 5 | The composition of the simulated artificial seawater solution

Compound	Concentration (g/L)
NaCl	24.53
$MgCl_2$	5.20
Na_2SO_4	4.09
$CaCl_2$	1.16
KCl	0.695
$NaHCO_3$	0.201
KBr	0.101
H_3BO_3	0.027
$SrCl_2$	0.025
NaF	0.03

(25 °C–3 MPa-1 m/s) were used to simulate the shutdown and operation of the B30 alloy heat-transfer tube in aggressive deep-sea environment. The static immersion test was conducted in a constant temperature water bath. The flow accelerated corrosion test was conducted in an autoclave with a rotating cage, whose details have been depicted in our previous publication[90]. The solution used in the corrosion tests was simulated artificial seawater, which was prepared using analytical-grade reagents and distilled water. Its composition meets the specifications of ASTM D1141–98[91], as shown in Table 5. After 30 days of corrosion test, according to the provisions of ASTM standard G1–03[92], the samples were descaled in a 1000 mL solution prepared by adding 50 g aminosulfonic acid and residual distilled water at room temperature to remove the corrosion products. The localized corrosion was observed using an Olympus confocal laser scanning microscope (CLSM, OLS4100, Japan). Then, the cumulative probability of localized corrosion pit depth was calculated according to the method in our previous publication[14].

Electrochemical measurements

All electrochemical measurements were conducted on a Princeton Electrochemical Workstation (Ametek, USA) connected to a typical three-electrode cell. The working electrodes were prepared by first welding copper leads to the back of the samples, and then sealing them with epoxy resin to ensure an exposed surface area of 1 cm^2. Platinum foil was used as the counter electrode, and a saturated calomel electrode as the reference electrode. The open-circuit potential (OCP) shall be monitored for 30 min before all electrochemical measurements to ensure that the system reaches a steady state. After pre-passivation treatment, the corrosion resistance of the passivation film was evaluated by potentiodynamic polarization curve. The scanning range was −0.3 V vs. OCP to +1.6 V vs. Ref. and the scanning rate of 0.333 mV/s. Electrochemical impedance spectroscopy (EIS) measurements under OCP were measured by applying a sinusoidal potential perturbation of 10 mV with a frequency range from 100 mHz to 10 kHz. The EIS data were fitted using ZSimpWin software. All electrochemical measurements were conducted in simulated artificial seawater at 25°C and repeated at least three times until the data were reproducible.

Microstructural characterization

The surface and cross-sectional morphologies of samples after pre-passivation treatment and corrosion tests were characterized using scanning electron microscopy (SEM, FEI Quanta 200 F, USA), and the elemental compositions were analyzed by EDS. Before characterizing the cross-sectional morphology, the cross-section of the B30 alloy was ground to 5000 grit, and then argon ion etching was performed to achieve a smooth, stress-free surface. The microstructure of passivation films was analyzed by transmission electron microscopy (TEM, FEI Tecnai G20, USA) and SAED. TEM samples were prepared using a dual-beam focused ion beam at an accelerating voltage of 30 kV after deposition of a Pt layer to protect the film surface. XPS was used to analyze the composition of the passivation film. Peak identification was performed using CasaXPS software using an XPS database as a reference. The binding energy scale was calibrated to the C 1 s peak at 284.8 eV. Moreover, TOF-SIMS was used to determine the composition distribution of the film.

Data availability

Data will be made available from the corresponding author on request.

Received: 12 June 2025; Accepted: 11 September 2025;
Published online: 04 November 2025

References

1. Shen, M. J., Zhang, F., Liu, Y. S. & Zhou, X. P. Molecular dynamics study on the viscosity of hydraulic oil in the deep-sea environment. *J. Mol. Liq.* **411**, 125716 (2024).
2. Ren, P. W., Meng, H. M., Xia, Q. J., Zhu, Z. Z. & He, M. T. Tribocorrosion of 316L stainless steel by in-situ electrochemical methods under deep-sea high hydrostatic pressure environment. *Corros. Sci.* **202**, 110315 (2022).
3. Faes, W. et al. Corrosion and corrosion prevention in heat exchangers. *Corros. Rev.* **37**, 131–155 (2019).
4. Lu, J. C., Wang, Z. B., Hu, H. X. & Zheng, Y. G. Understanding localized corrosion mechanism of 90/10 copper-nickel alloy in flowing NaCl solution induced by partial coverage of corrosion products films. *Corros. Sci.* **227**, 111716 (2024).
5. Jin, T. Z. et al. Surface characterization and corrosion behavior of 90/10 copper-nickel alloy in marine environment. *Materials* **12**, 1869 (2019).
6. Ma, A. L., Jiang, S. L., Zheng, Y. G. & Ke, W. Corrosion product film formed on the 90/10 copper-nickel tube in natural seawater: Composition/structure and formation mechanism. *Corros. Sci.* **91**, 245–261 (2015).
7. Ismail, K. M., Fathi, A. M. & Badawy, W. A. Effect of nickel content on the corrosion and passivation of copper-nickel alloys in sodium sulfate solutions. *Corrosion* **60**, 795–803 (2004).
8. Burleigh, T. D. & Waldeck, D. H. Effect of alloying on the resistance of Cu-10% Ni alloys to seawater impingement. *Corrosion* **55**, 800–804 (1999).
9. Zhu, Y. B. et al. Effect of iron on the composition and structure of corrosion product film formed in 70/30 copper-nickel alloy. *Anti-Corros. Methods Mater.* **68**, 113–121 (2021).
10. Wu, L. et al. Effect of pre-immersion temperature on corrosion product films and their erosion corrosion resistance on 90/10 and 70/30 copper-nickel tubes in 1 wt.% NaCl solution. *J. Mater. Eng. Perform.* **8**, 2567–2584 (2024).
11. Kuznicka, B. Erosion-corrosion of heat exchanger tubes. *Eng. Fail. Anal.* **16**, 2382–2387 (2009).
12. Chandra, K., Kain, V., Dey, G. K., Shetty, P. S. & Kishan, R. Failure analysis of cupronickel evaporator tubes of a chilling plant. *Eng. Fail. Anal.* **17**, 587–593 (2010).
13. Yuan, S. J. & Pehkonen, S. O. Surface characterization and corrosion behavior of 70/30 Cu-Ni alloy in pristine and sulfide-containing simulated seawater. *Corros. Sci.* **49**, 1276–1304 (2007).
14. Yin, T. F. et al. Investigation of an efficient pre-immersion treatment of B30 alloy used for power systems in an aggressive deep-sea environment. *Corros. Sci.* **251**, 112925 (2025).
15. Cheng, Y. L., Zhu, Z. D., Zhang, Q. H., Zhuang, X. J. & Cheng, Y. L. Plasma electrolytic oxidation of brass. *Surf. Coat. Technol.* **385**, 125366 (2020).
16. Zhao, Y., Li, Y. B., Yin, T. F., Zhang, T. & Wang, F. H. Investigation of the post-treatment process for improving corrosion behaviors and adhesion strength of plasma electrolytic oxidation (PEO) coatings on pure copper. *Surf. Coat. Technol.* **472**, 129873 (2023).
17. Xin, J. M. et al. Corrosion resistance and formation mechanism of oxide film formed on 70Cu-30Ni alloy under different pre-filming processes. *Appl. Surf. Sci.* **689**, 162503 (2025).

18. North, R. F. & Pryor, M. J. The protection of Cu by ferrous sulphate additions. *Corros. Sci.* **8**, 149–157 (1968).
19. Chauhan, P. K. & Gadiyar, H. S. XPS study of the corrosion of Cu-10Ni alloy in unpolluted and polluted sea-water; The effect of $FeSO_4$ addition. *Corros. Sci.* **25**, 55–68 (1985).
20. Subramanian, V., Chandramohan, P., Srinivasan, M. P., Velmurugan, S. & Narasimhan, S. V. Corrosion of cupronickel alloy in permanganate under acidic condition. *Corros. Sci.* **49**, 620–636 (2007).
21. Ha, H. M. & Scully, J. R. Effects of phosphate on pit stabilization and propagation in copper in synthetic potable waters. *Corrosion* **69**, 703–718 (2013).
22. Wang, W. Y., Zhang, W. J., Huang, G. J., Mi, X. J. & Huang, L. Effect of in-situ pre-soaking in seawater on the erosion-corrosion properties and micro-mechanism of nickel aluminium bronze alloy. *Corros. Sci.* **228**, 111841 (2024).
23. Wu, L., Xu, Y. T., Ma, A. L., Zhang, L. M. & Zheng, Y. G. Influence of pre-immersion aeration conditions on corrosion product films and erosion-corrosion resistance of 90/10 and 70/30 copper-nickel tubes in 1 wt% NaCl solution. *Corros. Sci.* **228**, 111817 (2024).
24. Yang, T. et al. Environment-friendly and chromium-free passivation of copper and its alloys. *Mater. Today Commun.* **29**, 102826 (2021).
25. Li, W. et al. Insights into triazole derivatives as potential corrosion inhibitors in CMP process: Experimental evaluation and theoretical analysis. *Appl. Surf. Sci.* **602**, 154165 (2022).
26. Liao, C. F. et al. In situ observation and SKPFM analysis to study the adsorption behavior and corrosion inhibition mechanism of 2-aminobenzimidazole inhibitor on Cu-5 wt% Fe alloys. *Appl. Surf. Sci.* **687**, 162232 (2025).
27. Benmessaoud, M. et al. Inhibiting effect of 2-mercaptobenzimidazole on the corrosion of Cu–30Ni alloy in aerated 3% NaCl in presence of ammonia. *Corros. Sci.* **49**, 3880–3888 (2007).
28. Ukaga, I., Okafor, P., Onyeachu, I. B., Ikeuba, A. I. & Njoku, D. I. The inhibitive performance of 2,3-pyrazine dicarboxylic acid and synergistic impact of KI during acid corrosion of 70/30 and 90/10 copper–nickel alloys. *Mater. Chem. Phys.* **296**, 127313 (2023).
29. Xu, F. L. et al. Thiol self-assemble layer as inhibitor to protect B10 from seawater corrosion. *Prog. Org. Coat.* **97**, 82–90 (2016).
30. Finsgar, M. & Merl, D. K. 2-Mercaptobenzoxazole as a copper corrosion inhibitor in chloride solution: Electrochemistry, 3D-profilometry, and XPS surface analysis. *Corros. Sci.* **80**, 82–95 (2014).
31. El-Egamy, S. S. Corrosion and corrosion inhibition of Cu–20%Fe alloy in sodium chloride solution. *Corros. Sci.* **50**, 928–937 (2008).
32. Wu, T. X., Gao, B. H., Zheng, Q., Liu, S. T. & Wang, J. Corrosion inhibition and the synergistic effect of three different inhibitors on copper surface. *ECS J. Solid State Sci. Technol.* **11**, 054009 (2022).
33. Onyeachu, I. B., Solomon, M. M., Umoren, S. A., Obot, I. B. & Sorour, A. A. Corrosion inhibition effect of a benzimidazole derivative on heat exchanger tubing materials during acid cleaning of multistage flash desalination plants. *Desalination* **479**, 114283 (2020).
34. Sun, S. Q. Density functional theory study of imidazole, benzimidazole and 2-mercaptobenzimidazole adsorption onto clean Cu (111) surface. *Corros. Sci.* **62**, 140–147 (2012).
35. Finsgar, M. & Milosev, I. Inhibition of copper corrosion by 1,2,3-benzotriazole: a review. *Corros. Sci.* **52**, 2737–2749 (2010).
36. Johar, M. H., Torbati-Sarraf, H., Ahangari, M. & Saremi, M. Inhibiting effect of Benzotriazole on the stress corrosion cracking of Cu-27%Ni cupronickel and Cu-30%Zn brass in Mattsson's solution. *Mater. Lett.* **293**, 129735 (2021).
37. Gerengi, H., Darowicki, K., Bereket, G. & Slepski, P. Evaluation of corrosion inhibition of brass-118 in artificial seawater by benzotriazole using Dynamic EIS. *Corros. Sci.* **51**, 2573–2579 (2009).
38. Ma, X. Z. et al. Synergistic inhibition of azoles compounds on chloride-induced atmospheric corrosion of copper: Experimental and theoretical characterization. *Corros. Sci.* **218**, 111161 (2023).
39. Kosec, T., Merl, D. K. & Milosev, I. Impedance and XPS study of benzotriazole films formed on copper, copper-zinc alloys and zinc in chloride solution. *Corros. Sci.* **50**, 1987–1997 (2008).
40. Tromans, D. Aqueous potential-pH equilibria in copper-benzotriazole systems. *J. Electrochem. Soc.* **145**, 42–45 (1998).
41. Lei, Y., Sheng, N., Hyono, A., Ueda, M. & Ohtsuka, T. Effect of benzotriazole (BTA) addition on Polypyrrole film formation on copper and its corrosion protection. *Prog. Org. Coat.* **77**, 339–346 (2014).
42. Wan, S., Miao, C. H., Wang, R. M., Zhang, Z. F. & Dong, Z. H. Enhanced corrosion resistance of copper by synergetic effects of silica and BTA codoped in polypyrrole film. *Prog. Org. Coat.* **129**, 187–198 (2019).
43. Villamil, R. F. V., Cordeiro, G. G. O., Matos, J., D'Elia, E. & Agostinho, S. M. L. Effect of sodium dodecylsulfate and benzotriazole on the interfacial behavior of Cu/Cu(II), H_2SO_4. *Mater. Chem. Phys.* **78**, 448–452 (2002).
44. Villamil, R. F. V., Corio, P., Rubim, J. C. & Agostinho, S. M. L. Effect of sodium dodecylsulfate on copper corrosion in sulfuric acid media in the absence and presence of benzotriazole. *J. Electroanal. Chem.* **472**, 112–119 (1999).
45. Liao, X., Huang, R. J., Zhu, D. C. & Yan, Q. Influence of benzotriazole and cerium chloride on anticorrosion performance of Cu-0.25Se-0.25Te alloy in 3.5 wt% NaCl solution. *Corrosion* **76**, 570–577 (2020).
46. Wang, Y. Q., Shao, Y. W., Meng, G. Z., Zhang, T. & Wang, F. H. Study on passivating treatment of Cu-Ni alloy in compound passivant containing benzotriazole. *Acta Metall. Sin* **48**, 744–748 (2012).
47. Yin, T. F., Meng, S., Zhao, Y., Zhang, T., Wang, F. H. Modeling of the corrosion behavior of B30 alloy in a deep-sea environment by using the response surface methodology. *Mater. Corros*. **75**, 174–187 (2023).
48. Kosec, T., Milosev, I. & Pihlar, B. Benzotriazole as an inhibitor of brass corrosion in chloride solution. *Appl. Surf. Sci.* **253**, 8863–8873 (2007).
49. Gao, H. Y., Liang, Z. P., Wang, Y. Y. & Jin, H. Study of initial corrosion and protection behavior of bronze from the Western Zhou Dynasty assisted by BTA. *Corros. Sci.* **239**, 112419 (2024).
50. Muresan, L. et al. Protection of bronze covered with patina by innoxious organic substances. *Electrochim. Acta* **52**, 7770–7779 (2007).
51. Rahmouni, K., Takenouti, H., Najjaji, N., Srhiri, A. & Robbiola, L. Protection of ancient and historic bronzes by triazole derivatives. *Electrochim. Acta* **54**, 5206–5215 (2009).
52. Balbo, A., Chiavari, C., Martini, C. & Monticelli, C. Effectiveness of corrosion inhibitor films for the conservation of bronzes and gilded bronzes. *Corros. Sci.* **59**, 204–212 (2012).
53. Laguzzi, G. & Luvidi, L. Evaluation of the anticorrosive properties of benzotriazole alkyl derivatives on 6% Sn bronze alloy. *Surf. Coat. Technol.* **204**, 2442–2446 (2010).
54. Chen, J. C. & Tsai, W. T. Effects of hydrogen peroxide and alumina on surface characteristics of copper chemical-mechanical polishing in citric acid slurries. *Mater. Chem. Phys.* **87**, 387–393 (2004).
55. Jiang, L., He, Y. Y., Li, J. & Luo, J. B. Passivation kinetics of 1,2,4-Triazole in copper chemical mechanical polishing. *ECS J. Solid State Sci. Technol.* **5**, 272–279 (2016).
56. Li, J., Liu, Y. H., Pan, Y. & Lu, X. C. Chemical roles on Cu-slurry interface during copper chemical mechanical planarization. *Appl. Surf. Sci.* **293**, 287–292 (2014).
57. Du, T., Tamboli, D., Desai, V. & Seal, S. Mechanism of copper removal during CMP in acidic H_2O_2 Slurry. *J. Electrochem. Soc.* **151**, 230–235 (2004).
58. Lin, J. Y. & Chou, S. W. Synergic effect of benzotriazole and chloride ion on Cu passivation in a phosphate electrochemical mechanical planarization electrolyte. *Electrochim. Acta* **56**, 3303–3310 (2011).
59. Choi, S., Dornfeld, D. A. & Doyle, F. M. Influence of copper ion concentration on the kinetics of formation of a protective layer on

copper in an acidic CMP solution containing BTA and glycine. *J. Electrochem. Soc.* **160**, 653–658 (2013).
60. Kondoh, E. et al. Structures of Cu surfaces developing in benzotriazole solutions: Effect of pH. *Jpn. J. Appl. Phys.* **56**, 07KH01 (2017).
61. Chen, J. C., Lin, S. R. & Tsai, W. T. Effects of oxidizing agent and hydrodynamic condition on copper dissolution in chemical mechanical polishing electrolytes. *Appl. Surf. Sci.* **233**, 80–90 (2004).
62. Jiang, L. 1,2,4-Triazole as a corrosion inhibitor in copper chemical mechanical polishing. *Thin Solid Films* **556**, 395–404 (2014).
63. Wang, Q. et al. Study on the adsorption and inhibition mechanism of 1,2,4-Triazole on copper surface in copper interconnection CMP. *ECS J. Solid State Sci. Technol.* **8**, 313–318 (2019).
64. Wang, Y. L., Liu, Y. C., Yang, Z. S. & Zhao, G. C. Electrochemical cleavage of DNA in the presence of copper-sulfosalicylic acid complex. *Bioelectrochemistry* **65**, 77–81 (2004).
65. Hayon, J., Yarnitzky, C., Yahalom, J. & Bettelheim, A. Surface processes characterization for the corrosion of copper in borate solutions. *J. Electrochem. Soc.* **149**, 314–320 (2002).
66. Gopi, D., Sherif, E. M., Surendiran, M., Angeline Sakila, D. M. & Kavitha, L. Corrosion inhibition by benzotriazole derivatives and sodium dodecyl sulphate as corrosion inhibitors for copper in ground water at different temperatures. *Surf. Interface Anal.* **47**, 618–625 (2015).
67. Pan, Y., Lu, X. C., Pan, G. S., Liu, Y. H. & Luo, J. B. Performance of sodium dodecyl sulfate in slurry with glycine and hydrogen peroxide for copper-chemical mechanical polishing. *J. Electrochem. Soc.* **157**, 1082–1087 (2010).
68. Cui, Y. N., Zhang, T. & Wang, F. H. New understanding on the mechanism of organic inhibitors for magnesium alloy. *Corros. Sci.* **198**, 110118 (2022).
69. Yohai, L., Schreiner, W. H., Vazquez, M. & Valcarce, M. B. Brass corrosion in chlorinated tap water inhibited by phosphate ions. *J. Solid State Electrochem.* **19**, 1559–1568 (2015).
70. Zhang, Y. et al. Corrosion behavior and passive film properties of nickel-based alloy in phosphoric acid. *Corros. Commun.* **9**, 77–88 (2023).
71. Guo, S. W., Xu, D. H., Jiang, G. Y., Guo, Y. & Jing, Z. F. Sulfate corrosion and phosphate passivation of Ni-based alloy in supercritical water. *J. Supercrit. Fluids* **184**, 105564 (2022).
72. Kim, N. H., Lim, J. H., Kim, S. Y. & Chang, E. G. Effects of phosphoric acid stabilizer on copper and tantalum nitride CMP. *Mater. Lett.* **57**, 4601–4604 (2003).
73. Miranda-Alcantara, B., Bonola, B., Vazquez-Arenas, J. & Rivera, F. Optimization of active chlorine production in a filter-press type electrochemical reactor through continuum modelling and response surface methodology. *J. Electrochem. Soc.* **171**, 043505 (2024).
74. Ye, S. et al. Rapid planarization of polycrystalline diamond by laser with response surface methodology. *Opt. Laser Technol.* **180**, 111509 (2025).
75. Sun, Y. T. et al. Mechanisms of inclusion-induced pitting of stainless steels: a review. *J. Mater. Sci. Technol.* **168**, 143–156 (2024).
76. Wu, Y. H., Luo, S. X. & Mou, Q. S. Influence of temperature on the corrosion behavior of X80 steel in an acidic soil environment. *Int. J. Electrochem. Sci.* **15**, 576–586 (2020).
77. Xia, S. et al. Effects of temperature on corrosion behavior of reinforcements in simulated sea-sand concrete pore solution. *Buildings* **12**, 407 (2022).
78. Taylor, C. D., Tossey, B. M. High temperature oxidation of corrosion resistant alloys from machine learning. *npj Mater. Degrad.* **5**, 38 (2021).
79. Emran, K. M., Omar, I. M. A., Arab, S. T. & Ouerfelli, N. On the pseudo-hyperbolic behavior of charge transfer resistance-temperature dependence in corrosion behavior of Nickel based glass alloy. *Sci. Rep.* **12**, 6432 (2022).
80. Milosev, I. & Metikos-Hukovic, M. Effect of chloride concentration range on the corrosion resistance of Cu-xNi alloys. *J. Appl. Electrochem.* **29**, 393–402 (1999).
81. Ling, Y., Guan, Y. & Han, K. N. Corrosion inhibition of copper with benzotriazole and other organic surfactants. *Corrosion* **51**, 367–375 (1995).
82. Finsgar, M., Kovac, J. & Milosev, I. Surface analysis of 1-hydroxybenzotriazole and benzotriazole adsorbed on Cu by X-ray photoelectron spectroscopy. *J. Electrochem. Soc.* **157**, 52–60 (2010).
83. Allam, N. K., Nazeer, A. A. & Ashour, E. A. A review of the effects of benzotriazole on the corrosion of copper and copper alloys in clean and polluted environments. *J. Appl. Electrochem.* **39**, 961–969 (2009).
84. Wang, R. G. et al. Microstructure of Ni-based hard facing alloy and its polarization behavior in aqueous solution with different pH and chloride concentration. *Corros. Commun.* **3**, 1–9 (2021).
85. Zhao, Y., Zhang, T., Xiong, H. & Wang, F. H. Bridge for the thermodynamics and kinetics of electrochemical corrosion: Modeling on dissolution, ionization, diffusion and deposition in metal/solution interface. *Corros. Sci.* **191**, 109763 (2021).
86. Zhou, Z. et al. Formation and corrosion behavior of Fe-based amorphous metallic coatings by HVOF thermal spraying. *Surf. Coat. Technol.* **204**, 563–570 (2009).
87. Zheng, Z. B., Zheng, Y. G., Sun, W. H. & Wang, J. Q. Effect of applied potential on passivation and erosion-corrosion of a Fe-based amorphous metallic coating under slurry impingement. *Corros. Sci.* **82**, 115–124 (2014).
88. Zhao, Y. et al. Effect of the flow velocity on the corrosion behavior of UNS S41426 stainless steel in the extremely aggressive oilfield environment for the Tarim area. *Corrosion* **76**, 654–665 (2020).
89. Koch, P. N., Mavris, D. & Mistree, F. Partitioned, multilevel response surfaces for modeling complex systems. *AIAA J.* **38**, 875–881 (2000).
90. Zhao, Y. et al. Investigation of the rotation speed on corrosion behavior of HP-13Cr stainless steel in the extremely aggressive oilfield environment by using the rotating cage test. *Corros. Sci.* **145**, 307–319 (2018).
91. ASTM. Standard D1141-98, Standard Practice for the Preparation of Substitute Ocean Water, ASTM International, West Conshohocken, PA, 2013.
92. ASTM. Standard G1-03, Standard Practice for Preparing Cleaning and Evaluating Corrosion Test Specimens, ASTM International, West Conshohocken, PA, 2003.

Acknowledgements

This work was financially supported by the Program of the National Natural Science Foundation of China (52371055), the Liaoning Province Science and Technology Plan Joint Program (Applied Basic Research Project) (2023JH2/101700305), the Hubei Province Key Laboratory of Systems Science in Metallurgical Process (Wuhan University of Science and Technology) (Y202404), the basic scientific research project of Liaoning provincial department of education (JYTMS20230618) and the Fundamental Research Funds for the Central Universities (2024GFYD01 and N2402004). Special thanks are due to the instrumental analysis from the Analytical and Testing Centre, Northeastern University.

Author contributions

This work was conceived by T.Y. and S.M. T.Y. wrote the original draft, reviewed by Y.Z. Y.Z., T.Z., and F.W. contributed to funding acquisition and project management. Both authors approved the final version.

Competing interests
The authors declare no competing interests.

Additional information
Supplementary information The online version contains supplementary material available at https://doi.org/10.1038/s41529-025-00674-8.

Correspondence and requests for materials should be addressed to Yang Zhao.